

Groundwater affects the geomorphic and hydrologic properties of coevolved landscapes

David Litwin¹, Gregory E. Tucker², Katherine R. Barnhart³, and Ciaran J Harman¹

¹Johns Hopkins University

²University of Colorado Boulder

³U.S. Geological Survey

May 05, 2021

Abstract

The hydrologic dynamics and geomorphic evolution of watersheds are intimately coupled – runoff generation and water storage are controlled by topography and properties of the surface and subsurface, while also affecting the evolution of those properties over geologic time. However, the large disparity between their timescales has made it difficult to examine interdependent controls on emergent hydro-geomorphic properties, such as hillslope length, drainage density, extent of surface saturation. In this study, we develop a new model coupling hydrology and landscape evolution to explore how runoff generation affects long-term catchment evolution, and analyze numerical results using a nondimensional scaling framework. We focus on hydrologic processes dominating in humid climates where storm runoff primarily arises from shallow subsurface flow and from precipitation on saturated areas. The model solves hydraulic groundwater equations to predict the water table location given prescribed, constant groundwater recharge. Water in excess of the subsurface capacity for transport becomes overland flow, which generates shear stress on the surface and may detach and transport sediment. This affects the landscape form that in turn affects runoff generation. We show that (1) three dimensionless parameters describe the possible steady state landscapes that coevolve under steady recharge; (2) hillslope length increases with increasing transmissivity relative to the recharge rate; (3) three topographic metrics—steepness index, Laplacian curvature, and topographic index—provide a basis to recover key model parameters from topography (including subsurface transmissivity). These results open possibilities for topographic analysis of humid upland landscapes that could inform quantitative understanding of hydrological processes at the landscape scale.

Abstract

The hydrologic dynamics and geomorphic evolution of watersheds are intimately coupled – runoff generation and water storage are controlled by topography and properties of the surface and subsurface, while also affecting the evolution of those properties over geologic time. However, the large disparity between their timescales has made it difficult to examine interdependent controls on emergent hydro-geomorphic properties, such as hillslope length, drainage density, extent of surface saturation. In this study, we develop a new model coupling hydrology and landscape evolution to explore how runoff generation affects long-term catchment evolution, and analyze numerical results using a non-dimensional scaling framework. We focus on hydrologic processes dominating in humid climates where storm runoff primarily arises from shallow subsurface flow and from precipitation on saturated areas. The model solves hydraulic groundwater equations to predict the water table location given prescribed, constant groundwater recharge. Water in excess of the subsurface capacity for transport becomes overland flow, which generates shear stress on the surface and may detach and transport sediment. This affects the landscape form that in turn affects runoff generation. We show that (1) three dimensionless parameters describe the possible steady state landscapes that coevolve under steady recharge; (2) hillslope length increases with increasing transmissivity relative to the recharge rate; (3) three topographic metrics—steepness index, Laplacian curvature, and topographic index—provide a basis to recover key model parameters from topography (including subsurface transmissivity). These results open possibilities for topographic analysis of humid upland landscapes that could inform quantitative understanding of hydrological processes at the landscape scale.

1 Introduction**1.1 Motivation**

Landscape morphology and subsurface structure are strong predictors of runoff generation style and spatial distribution (Dunne, 1978). In humid climates, the infiltration capacity of undisturbed soil is high and overland flow due to exceedance of soil infiltration capacity is rare. When relief is relatively low and soils are relatively thin, runoff is most commonly generated by the expansion of variable source areas, which may generate overland flow where precipitation falls directly on saturated areas (Dunne & Black, 1970). In steeper landscapes with deep soils, water may be transmitted laterally through the subsurface at permeability contrasts, becoming surface runoff only when it reaches stream channels (Hewlett & Hibbert, 1967). Saturated areas (including wetted stream channels) emerge as the supply of water from upslope areas exceeds the conveyance capacity of water through the subsurface. This competition between upslope supply and downslope transport capacity links properties of the subsurface, such as transmissivity, to the runoff response of watersheds as a whole (O’Loughlin, 1981). Furthermore, overland flow generates shear stress on the land surface that may detach and transport sediment. This drives the evolution of topographic convergence/divergence and convexity/concavity, which are important controls on runoff generation themselves (Prancevic & Kirchner, 2019; Troch et al., 2003; Lapides et al., 2020).

Research also suggests that incision and hillslope sediment transport play a role in setting the rate and extent of subsurface weathering by setting the rate at which fresh bedrock is supplied to the near surface (Gabet & Mudd, 2009; West et al., 2005). Subsurface weathering is in turn crucial for setting subsurface properties that affect groundwater flow and storage capacity. These feedbacks suggest that there should be intimate links between runoff generation behavior and landscape morphology. If morphology affects and is affected by runoff generation, how might long-term evolution set the extent of surface saturation in a landscape? Are there emergent relationships between topographic

68 form and shallow subsurface hydrology that we could quantify? Here we will draw in-
69 sights from coupled a coupled hydro-geomorphic model to answer these questions.

70 1.2 Background

71 Over geologic time, upland landscapes are shaped by the competition between in-
72 cision by overland flow, gravitationally-driven fluxes of sediment due to processes includ-
73 ing biogenic disturbance and frost heaving, and baselevel change (Howard, 1994). While
74 it is not possible to observe the evolution of landscapes at human timescales, numeri-
75 cal landscape evolution models (LEMs) have allowed researchers to make substantial progress
76 in understanding how landscapes respond to dynamic forcings of tectonics, lithology, and
77 climate (e.g., reviews by Chen et al., 2014; Bishop, 2007; Martin & Church, 2004; Pel-
78 letier, 2013; Pazzaglia, 2003; Temme et al., 2013; Valters, 2016). However, the treatment
79 of hydrology in models that consider evolution over geologic time remains rudimentary.

80 Early LEMs treated runoff as the product of upslope area and an effective precipi-
81 tation rate (Willgoose, Bras, & Rodriguez-Iturbe, 1991; Ahnert, 1976; Armstrong, 1976),
82 representing the time-averaged runoff from infiltration excess overland flow. In these mod-
83 els, all areas of the landscape generated surface runoff simultaneously, though all areas
84 may not experience erosion due to the presence of thresholds for sediment detachment
85 (Horton, 1945). The practice of using such runoff formulations in LEMs is still common
86 today when hydrologic response is not central to the study, as models with minimal hy-
87 drologic dynamics can still effectively capture certain essential aspects of landscape form
88 (e.g., Forte et al., 2016; Barnhart, Tucker, Doty, Glade, et al., 2020; Theodoratos et al.,
89 2018). One of the first attempts to capture subsurface hydrology in a LEM came when
90 Ijjász-Vásquez et al. (1992) developed a model that partitioned flow between surface and
91 subsurface using a steady state topographic index criterion (Beven & Kirkby, 1979). The
92 authors found that this partitioning significantly changed catchment hypsometry in com-
93 parison to the infiltration excess formulation. Tucker and Bras (1998) compared several
94 different landscape evolution and runoff generation formulations, including one that treats
95 subsurface transport capacity similarly to Ijjász-Vásquez et al. (1992). They found that
96 the evolved landscapes have sharp hillslope-valley transitions at a critical value of topo-
97 graphic index. These transitions were smoothed by treating precipitation as a random
98 process with an exponential distribution, rather than having a single value. However,
99 the topographic index type models neglect the role of nonlinearities in groundwater flow,
100 and antecedent conditions that determine catchment runoff response to precipitation.
101 Flow nonlinearity affects the degree to which groundwater flow is driven by diffusion of
102 the water table rather than advection due to slope gradients of permeability contrasts,
103 and can have significant effects on runoff generation (C. Harman & Sivapalan, 2009). The
104 steady state assumption of the topographic index model assumes that a storm event is
105 effectively independent of prior events, and arrives with the full subsurface capacity avail-
106 able to drain flow. Many hydrological studies have shown that antecedent conditions are
107 important controls on runoff magnitudes, where wetter systems are primed for larger runoff
108 response due to lack of available subsurface storage or transport capacity (Brocca et al.,
109 2009; Trambly et al., 2010).

110 Several studies have coupled landscape evolution with hydrological processes in greater
111 detail. Huang and Niemann (2006, 2008) developed a coupled groundwater model and
112 LEM, and demonstrated the importance of dynamic runoff generation mechanisms for
113 the topographic evolution of different areas of modeled basins. Huang and Niemann (2006)
114 focused on the evolution of a single well-studied catchment, and found that as they sim-
115 ulated its evolution from present, runoff was increasingly generated by subsurface lat-
116 eral flow rather than saturation excess overland flow. Huang and Niemann (2008) ex-
117 plored the long-term geomorphic evolution of synthetic catchments with groundwater
118 flow, and concluded that the hypsometry of steady state landscapes was not generally
119 distinguishable between surface-water-dominated and groundwater-dominated landscapes.

120 In this case, sensitivity of modeled topography to parameters was conducted by impos-
 121 ing changes on the slope-area relationship rather than examining results of the coupled
 122 model, making it more difficult to evaluate the precise role of groundwater flow in long
 123 term evolution. Zhang et al. (2016) presented a highly detailed, coupled hydrological model
 124 and LEM, though to our knowledge it has not been used beyond the initial proof of con-
 125 cept. With solutions to Richards equation for subsurface flow and St. Venant’s equation
 126 for surface flow and employment of several dozen parameters, this model is computationally
 127 expensive and may be more complex than needed to explore process feedbacks be-
 128 tween shallow subsurface hydrology and landscape evolution. A systematic approach is
 129 needed to understand these feedbacks. It must be simple enough for interpretation of
 130 process controls while still having the core elements of landscape evolution and dynamic
 131 runoff generation from the shallow subsurface.

132 1.3 Approach

133 In this study, we develop and use a new groundwater-landscape evolution model
 134 to explore how subsurface-mediated runoff generation affects long-term catchment evo-
 135 lution. The model solves hydraulic groundwater equations to predict the water table lo-
 136 cation given prescribed recharge. Water in excess of the subsurface flow capacity becomes
 137 overland flow, which may detach and transport sediment, altering topographic proper-
 138 ties that in turn affect runoff generation. Our model can support recharge rates which
 139 vary in space and time, but here we constrain the scope to considering only steady, uni-
 140 form recharge. In order to generalize our understanding from the model results, we con-
 141 duct a similarity analysis that provides new insight into the dynamics behind the widely
 142 used “stream power plus diffusion” model by reconciling contradictory dimensional anal-
 143 yses provided by Theodoratos et al. (2018) and Bonetti et al. (2020). We can reduce the
 144 seven dimensional parameters of the model to four dimensionless parameters, one of which
 145 is always negligible. We present numerical results confirming the efficacy of our nondi-
 146 mensionalization and exploring the newly defined non-dimensional parameter space to
 147 determine how hydrologic and geomorphic parameters determine emergent hydro-geomorphic
 148 properties at geomorphic steady state. The results show that subsurface flow capacity
 149 relative to recharge rate exerts a fundamental control on hillslope length and relief, and
 150 that three topographic metrics derived from the governing equations form a natural ba-
 151 sis for evaluating the resulting coevolved landscapes. We derive and discuss a theoret-
 152 ical relationship between these metrics that allows us to recover the key model input pa-
 153 rameters (including subsurface transmissivity) from topographic analysis of the landscape.
 154 We conclude by discussing the possibilities this analysis may open for topographic anal-
 155 ysis of humid upland landscapes that could inform quantitative understanding of hydro-
 156 logical processes at the landscape scale.

157 2 Governing equations

158 To investigate the effects of subsurface hydrology on landscape evolution, we cou-
 159 ple a hydrological model to a standard model of landscape evolution. First, we derive
 160 a governing equation for topographic evolution that includes the role of space- and time-
 161 variable runoff in fluvial incision. Second, we examine the hydrological model that will
 162 generate runoff. Variable dimensions are provided in Sec. 9.

163 2.1 Landscape evolution

164 Topographic elevation $z(x, y, t)$ is assumed to evolve due to fluvial incision $E_f(x, y, t)$,
 165 hillslope diffusion $E_h(x, y, t)$, and constant baselevel change U .

$$\frac{\partial z}{\partial t} = -E_f - E_h + U \quad (1)$$

166 The term E_f accounts for incision into the landscape by erosion due to overland
 167 flow. The term E_h accounts for gravitational soil-transport processes that tend to smooth
 168 out landscape features. The term U accounts for the constant rate of either tectonic up-
 169 lift or baselevel fall, in this case increasing topographic elevation relative to a fixed el-
 170 evation boundary.

In one commonly used form of this equation, fluvial incision is described by the stream-
 power law, originally derived from empirical data (Howard & Kerby, 1983):

$$E_f = KA^m |\nabla z|^n \quad (2)$$

Here $A(x, y, t)$ is the upslope drainage area. In the standard streampower formulation,
 the exponents are $m = 1/2$ and $n = 1$. This is supported by observations of stream
 profile concavity that suggest $m/n \approx 0.5$, and a derivation in which incision is propor-
 tional to streampower per unit surface area, and channel width increases with the square
 root of discharge (Whipple & Tucker, 1999; Barnhart, Tucker, Doty, Shobe, et al., 2020).
 This gives the streampower incision law:

$$E_f = K\sqrt{A}|\nabla z| \quad (3)$$

171 This equation obscures the role of hydrological processes in the fluvial incision that
 172 drives landscape evolution. The relationship in (3) can also be derived from first prin-
 173 ciples in a way that provides a natural coupling to hydrological processes. This is accom-
 174 plished by assuming the incision rate E_f is related to the excess shear stress τ from over-
 175 land flow by some relationship. Frequently, this is written in the form:

$$E_f = k_e(\tau - \tau_c)^\beta \quad (4)$$

176 This excess shear stress formulation assumes that sediment is not redeposited within
 177 the domain (meaning that the system is assumed to be “detachment-limited”), which
 178 is widely used for upland watersheds (Howard, 1994). The shear stress generated by steady,
 179 uniform flow in a rectangular channel is:

$$\tau = \rho_w g d_f |\nabla z|, \quad (5)$$

180 where ρ_w is the density of water, g is the acceleration due to gravity, and d_f is the flow
 181 depth. A constitutive relation for flow resistance such as the Manning or Chezy equa-
 182 tion can provide the flow depth d_f at a particular discharge Q . We use the Chezy equa-
 183 tion for simplicity, which gives:

$$d_f = \left(\frac{Q}{Cw\sqrt{|\nabla z|}} \right)^{2/3} \quad (6)$$

Here we assume that the channel width w is proportional to the square root of up-
 slope area (e.g., Snyder et al., 2003; Wohl & David, 2008):

$$w \sim \sqrt{A} \quad (7)$$

184 As we will show in subsequent scaling analysis, it will be useful to express this re-
 185 lation in terms of area per contour width $a(x, y, t)$. However, the hydraulic scaling re-
 186 lationships for channel width are defined on the basis of catchment area A at a given cross
 187 section (Leopold & Maddock, 1953). To make the conversion between A and a , we rep-
 188 resent A as the product of a and a characteristic contour width v_0 , which is a chosen con-
 189 stant value. We will examine the physical significance of this parameter in later sections.

190 To obtain values for w from the expression (7) we additionally require the dimension-
 191 less parameter k_w :

$$w = k_w \sqrt{v_0 a} \quad (8)$$

192 In this equation there is only one degree of freedom, so we are free to choose a value
 193 of v_0 for which there will always be a corresponding value of k_w to satisfy a given rela-
 194 tionship between a and w . Ultimately, k_w will become a component of the streampower
 195 coefficient K , while here v_0 remains separate, and has additional significance in the con-
 196 text of hydrological processes.

197 Next, we write the discharge $Q(x, y, t)$ as the product of an instantaneous runoff
 198 ratio $Q^*(x, y, t)$, upslope area A , and the average recharge rate p , $Q = pAQ^*$, and sub-
 199 stitute into (5) and (6) to find the flow depth and shear stress.

$$d_f = \left(\frac{Q^* p \sqrt{v_0 a}}{C k_w \sqrt{|\nabla z|}} \right)^{2/3} \quad (9)$$

$$\tau = \rho_w g \left(\frac{Q^* p \sqrt{v_0 a}}{C k_w \sqrt{|\nabla z|}} \right)^{2/3} |\nabla z| \quad (10)$$

200 To recover the the stream power formulation of the fluvial incision term, we set $\beta =$
 201 $3/2$ (Tucker, 2004) in (4), representative of hydraulic detachment by plucking (Whipple
 202 et al., 2000; Tsujimoto, 1999). With these substitutions, the incision rate E_f can be writ-
 203 ten as:

$$E_f = K \sqrt{v_0} Q^* \sqrt{a} |\nabla z| \quad (11)$$

204 where $K = \frac{(\rho_w g)^{3/2} k_e p}{C k_w}$. This form is equivalent to (3), with time and space varying runoff
 205 accounted for in Q^* . Additionally because Q^* is dimensionless, K in (11) has units of
 206 $[1/T]$, the same as in (3).

207 The upslope area A is usually defined by explaining the algorithms used to calcu-
 208 late it in numerical schemes, which find flow directions on a discrete grid and sum the
 209 grid cell areas downslope along these flow directions. However, this approach gives the
 210 area an implicit dependence on grid cell spacing. Area per contour width a on the other
 211 hand has a precise mathematical definition that can be derived from conservation of mass
 212 (Bonetti et al., 2018, 2020). Consider the steady state depth of water h_f across a sur-
 213 face where all locations contribute runoff at the same rate r . Conservation of mass for
 214 this system indicates that $\nabla \cdot (h_f u) = r$, where u is the (vector) flow velocity. Now sup-
 215 pose that the flow velocity at every point also has magnitude r and points in the direc-
 216 tion of steepest descent $-\nabla z / |\nabla z|$. To satisfy continuity with this velocity, the flow depth
 217 must be equal to the upslope area per contour width, $h_f = a$ (Bonetti et al., 2018). This
 218 derivation shows that, by definition:

$$-\nabla \cdot \left(a \frac{\nabla z}{|\nabla z|} \right) = 1 \quad (12)$$

219 We are not implying that the assumptions we have made here are necessarily char-
 220 acteristics of all real flow; rather these assumptions can be employed, without violating
 221 conservation of mass, to derive an expression for area per contour width as a function
 222 of the local terrain. This expression will become important in our scaling analysis in later
 223 sections, as the scaling properties of the governing equations should be independent of
 224 the numerical implementation where a grid cell width must be chosen.

225 Here we use a linear diffusion model of hillslope processes for E_h , which emerges
 226 by assuming that the non-fluvial sediment transport rate q_h is proportional to the local
 227 slope gradient $-\nabla z$, much as diffusion of a solute is proportional to the concentra-
 228 tion gradient (Dietrich et al., 2003). Then by assuming $E_h \sim -\nabla \cdot q_h$ from continuity,
 229 we find:

$$E_h = D\nabla^2 z, \quad (13)$$

230 where D is the linear diffusion constant. While nonlinear formulations of diffusion have
 231 proven useful in explaining topography (Roering et al., 1999; Roering, 2008), here we
 232 use linear diffusion to limit model complexity. We assume that baselevel change has a
 233 constant rate U in time and space by adopting a frame of reference anchored to base-
 234 level at the boundary of the domain. This can equivalently represent tectonic uplift or
 235 baselevel fall. This term becomes a “source” in the differential equation; without it, the
 236 topography would simply erode to a flat plane. While baselevel change is likely not steady
 237 in time in real landscapes, this assumption allows us to examine the emergent proper-
 238 ties of steady-state solutions to the governing equation. Combining all terms together,
 239 we arrive at our governing equations for topographic evolution:

$$\frac{\partial z}{\partial t} = -K\sqrt{v_0}Q^*\sqrt{a}|\nabla z| + D\nabla^2 z + U \quad (14)$$

$$-\nabla \cdot \left(a \frac{\nabla z}{|\nabla z|} \right) = 1 \quad (15)$$

240 This is different from the standard streampower formulation of landscape evolu-
 241 tion in that it includes a dimensionless runoff coefficient Q^* to account for the spatial
 242 and temporal variation in runoff across the landscape. While there is considerable un-
 243 certainty in the form of the fluvial incision term, the similarity between the form we have
 244 selected and the standard “stream power plus diffusion” formulation allows us to make
 245 use of the same nondimensionalization techniques used for the standard LEM, and has
 246 properties that will aid in implementation and analysis of results while remaining plau-
 247 sible within the context of the existing literature.

248 2.2 Hydrology

249 Thus far, we have made no assumptions regarding the hydrology, instead introduc-
 250 ing $Q^* = Q/(pA)$. Any approach to representing hydrology could use the above equa-
 251 tions by calculate appropriate values for Q^* . In our application surface water runoff is
 252 assumed to be generated by exfiltrating subsurface lateral flow (Hewlett & Hibbert, 1967)
 253 and by precipitation on saturated areas (Dunne & Black, 1970). We solve for this runoff
 254 using a quasi-3D shallow unconfined aquifer model using the Dupuit-Forchheimer approx-
 255 imations (e.g., Childs, 1971). This model makes use of a method of regularization intro-
 256 duced by Marçais et al. (2017) that greatly improves model stability at seepage faces.
 257 We solve the model for lateral groundwater flow $q(x, y, t)$, and local runoff production
 258 $q_s(x, y, t)$. Surface water discharge is calculated by instantaneously routing q_s and sum-
 259 ming the accumulated local runoff over the area upslope of a given location. The gov-
 260 erning equations for the hydrological model are:

$$\frac{\partial h}{\partial t} = \frac{1}{n} \left(p - \nabla \cdot q - q_s \right) \quad (16)$$

$$q = -h \cos \theta k_s (\nabla z + \nabla h) \cos \theta \quad (17)$$

$$q_s = \mathcal{G} \left(\frac{h}{b} \right) \mathcal{R} \left(i - \nabla \cdot q \right) \quad (18)$$

$$Q = \int_A q_s dA \quad (19)$$

261 where $h(x, y, t)$ is the aquifer thickness, n is the drainable porosity, $\theta(x, y, t)$ is the lo-
 262 cal slope of the (presumed impermeable) aquifer base, and b is the permeable thickness.
 263 The regularization function $\mathcal{G}(\cdot)$ has a value of zero when the argument is less than one,
 264 and approaches 1 as the argument approaches 1. The ramp function $\mathcal{R}(\cdot)$ is zero when
 265 the argument is less than zero and takes on the argument value when it is greater than
 266 zero.

267 Though this model can accommodate time-variable recharge, here we consider only
 268 constant recharge at rate p . Careful examination of this model reveals that saturated
 269 areas receive “recharge” at the same rate as areas with deeper water tables. In reality,
 270 saturated areas receive direct precipitation, while areas with deeper water tables receive
 271 a smaller fraction as a result of losses to unsaturated zone storage and evapotranspira-
 272 tion from the root zone. When saturated area is a small proportion of the total area and
 273 the water table is not too deep, this effect may be negligible. We will leave further in-
 274 vestigation on the role of unsaturated zone dynamics to a future contribution, as this
 275 would add considerable complexity to the model.

276 In the cases modeled here, the permeable thickness b is treated as constant in space
 277 and time. Considerable uncertainty exists in the rates and mechanisms that convert fresh
 278 bedrock to permeable fractured rock and/or regolith. Many past models have used an
 279 exponential function for the production of regolith (e.g., Ahnert, 1976; Armstrong, 1976;
 280 Rosenbloom & Anderson, 1994; Tucker & Slingerland, 1997), where the production rate
 281 is a function of regolith thickness. At geomorphic steady state, both the rates of change
 282 of topographic elevation and unweathered bedrock elevation go to zero. For the latter
 283 to be the case, the regolith production rate must be equal to the uplift rate. When the
 284 uplift rate and regolith production coefficients are spatially uniform, regolith thickness
 285 must be also be uniform to satisfy this equilibrium. This suggests that it is reasonable
 286 to treat permeable thickness as steady and uniform across the model domain given that
 287 we are only concerned with steady state landforms in this paper.

288 3 Numerical implementation

289 3.1 Timescale considerations

290 One of the primary challenges in coupling a hydrological model with a landscape
 291 evolution model is the vast difference in process timescales. While the relevant timescale
 292 for storm runoff response may be on the order of hours or even minutes, landscape evo-
 293 lution processes can have characteristic timescales in the tens to thousands of years. It
 294 would be too computationally expensive to run models over geologic time using appro-
 295 priately small timesteps for stability and accuracy of the hydrological model. Zhang et
 296 al. (2016) identified two approaches to address this problem: online updating and offline
 297 updating. In the offline case, the hydrological model is run for many steps without up-
 298 dating topography, and then appropriately averaged discharge values are used to update
 299 topography over some larger geomorphic timestep. In contrast, online updating involves
 300 having a direct scaling between the hydrological timestep (e.g., one storm event) and the
 301 geomorphic timestep. Zhang et al. (2016) use an online approach, citing possible non-

302 uniqueness of solutions in the offline approach depending on the time between geomor-
 303 phic updates. Given that we consider only steady recharge in this paper, there should
 304 not be a significant difference between online and offline approaches given that the hy-
 305 drological state varies gradually, only in response to changing topography. Nonetheless,
 306 our approach can be considered online updating, as we scale the geomorphic timestep
 307 as k_{sf} times the hydrological timestep: $\Delta t_g = k_{sf} \Delta t_h$.

308 3.2 Model implementation

309 The groundwater and landscape evolution models described above were implemented
 310 as the DupuitLEM Python package, which makes extensive use of existing tools from the
 311 Python-based Earth surface modeling toolkit Landlab (Hobley et al., 2017; Barnhart,
 312 Hutton, et al., 2020). Landlab includes tools for creating grids, setting boundary con-
 313 ditions, handling input and output, along with a diverse range of process components
 314 that modify fields on Landlab grids according to physical laws. The groundwater model
 315 described above is implemented as a component in Landlab called `GroundwaterDupuitPercolator`
 316 (Litwin et al., 2020).

317 DupuitLEM can handle raster, hexagonal, and irregular grids, along with zero-flux
 318 and fixed-value boundary conditions. The model base class takes components that up-
 319 date the hydrological state via hydrological fluxes and changes in boundary conditions,
 320 update topography via fluvial incision and hillslope diffusion, and update topography
 321 and regolith thickness via baselevel change and regolith production. Here we use the DupuitLEM
 322 subclass `StreamPowerModel`, designed for use with the Landlab fluvial incision compo-
 323 nent `FastScapeEroder`, which solves a modified version of the FastScape algorithm (Braun
 324 & Willett, 2013).

325 The hydrological state is updated with a DupuitLEM `HydrologicalModel`. All hy-
 326 drological models solve for aquifer state and fluxes using the `GroundwaterDupuitPercolator`
 327 component. Surface water discharge is routed instantaneously using a D8 algorithm when
 328 the grid is a raster, or a steepest descent algorithm otherwise. In the case of steady recharge,
 329 we use the `HydrologicalModel` subclass `HydrologySteadyStreamPower`, which updates
 330 the surface water discharge by advancing the `GroundwaterDupuitPercolator`, finding
 331 surface flow directions including routing through topographic depressions, and accumu-
 332 lating q_s along flow directions to determine Q . With known area A and recharge rate
 333 p , we can calculate the runoff ratio $Q^* = Q/(pA)$ that appears in our streampower model,
 334 linking the hydrology to geomorphic evolution. We use a raster grid with dimensions 125x125,
 335 with three zero flux boundaries (right, left, top) and one fixed value boundary along the
 336 bottom of the model domain. The geomorphic timestep is kept constant at 45 years, while
 337 the hydrologic timestep varies as a multiple of the von Neumann stability criteria, tak-
 338 ing values from approximately four hours to three days. The adaptive timestep solver
 339 of the `GroundwaterDupuitPercolator` will further subdivide the timestep to meet sta-
 340 bility criteria, while surface flow is only routed at this interval.

341 4 Scaling and similarity

342 A similarity analysis of the governing equations illuminates their fundamental con-
 343 trols and will guide the investigation conducted in the rest of this paper. Here we use
 344 an approach based on the concept of symmetry groups (Barenblatt, 1996). In essence,
 345 we seek to identify the complete set of scaling transformations of the governing equa-
 346 tions under which the solutions are invariant, and then apply transformations to con-
 347 solidate or eliminate parameters. This is an alternative approach to arrive at a general
 348 form of the governing equations where parameters emerge in dimensionless groups that
 349 can be varied in numerical experiments. We will begin this process by considering the
 350 simplest version of the model without space or time variable hydrology, where $Q^*(x, y) =$
 351 1 everywhere. We will call this the *NoHyd* model. Theodoratos et al. (2018) determined

352 that there are unique characteristic scales for the vertical coordinate, the horizontal co-
 353 ordinate, and time h_g, ℓ_g, t_g that emerge from the streampower-linear diffusion landscape
 354 evolution equations. The comparable scales for our governing equation are slightly dif-
 355 ferent, as we use the area per contour width a as a state variable rather than using area
 356 A . Based on the analysis of Theodoratos et al. (2018), we can rewrite equations (14) and
 357 (15) in terms of these scales without changing the units of the state variables.

$$t_g \frac{\partial z}{\partial t} = -\sqrt{\ell_g} Q^* \sqrt{a} |\nabla z| + \ell_g^2 \nabla^2 z + h_g \quad (20)$$

$$-\nabla \cdot \left(a \frac{\nabla z}{|\nabla z|} \right) = 1 \quad (21)$$

358 Because we have replaced three parameters, K , D , and U , with three characteristic scales
 359 h_g, ℓ_g , and t_g , without changing the state variables, we can solve for the three charac-
 360 teristic scales in terms of the model parameters:

$$h_g = \left(\frac{DU^3}{v_0^2 K^4} \right)^{1/3} \quad (22)$$

$$\ell_g = \left(\frac{D^2}{v_0 K^2} \right)^{1/3} \quad (23)$$

$$t_g = \left(\frac{D}{v_0^2 K^4} \right)^{1/3} \quad (24)$$

361 A physical law should remain valid regardless of the units that quantities are ex-
 362 pressed in. This endows physical laws with certain symmetries under scaling of the di-
 363 mensioned variables. There are three ways to scale two or more dimensioned variables
 364 by an arbitrary factor $c > 0$ that leave equations (20) and (21) unchanged.

$$\{t \rightarrow ct, t_g \rightarrow ct_g\} \quad (25)$$

$$\{z \rightarrow cz, h_g \rightarrow ch_g\} \quad (26)$$

$$\{x \rightarrow cx, y \rightarrow cy, a \rightarrow ca, \ell_g \rightarrow c\ell_g\} \quad (27)$$

365 Note that the final transformation also requires that $\nabla^2 z \rightarrow c^{-2} \nabla^2 z$ and $|\nabla z| \rightarrow$
 366 $c^{-1} |\nabla z|$, which are a consequence of the first two elements of the transformation.

367 These transformations can be applied as many times as desired, in any order, for
 368 any $c > 0$, and the equations remain the same because the factors c will always can-
 369 cel. For this reason, we can also choose values of c such that the characteristic scales do
 370 not appear in the equations. For example, we can apply the first transformation, tak-
 371 ing $c = 1/t_g$, we have the transformation $\{t \rightarrow t/t_g, t_g \rightarrow 1\}$. By doing this, we have
 372 effectively rescaled t into units relative to t_g . We will call this new time $t' = t/t_g$. Like-
 373 wise, we can do this with the other transformations:

$$\begin{aligned} &\{t \rightarrow t/t_g, t_g \rightarrow 1\} \\ &\{z \rightarrow z/h_g, h_g \rightarrow 1\} \\ &\{x \rightarrow x/\ell_g, y \rightarrow y/\ell_g, a \rightarrow a/\ell_g, \ell_g \rightarrow 1\} \end{aligned} \quad (28)$$

We apply all three transformations to define dimensionless state variables:

$$\begin{aligned}
 t' &= t/t_g \\
 z' &= z/h_g \\
 x' &= x/\ell_g \\
 y' &= y/\ell_g \\
 \nabla' &= \nabla \ell_g \\
 a' &= a/\ell_g
 \end{aligned}
 \tag{29}$$

and express the governing equations for the landscape evolution model:

$$\frac{\partial z'}{\partial t'} = -\sqrt{a'} |\nabla' z'| + \nabla'^2 z' + 1
 \tag{30}$$

$$-\nabla' \cdot \left(a' \frac{\nabla' z'}{|\nabla' z'|} \right) = 1
 \tag{31}$$

374 No parameters appear in these rescaled equations. This would not be the case if
 375 we had chosen to write the equations in terms of area A and not area per unit contour
 376 width a , as a single parameter of v_0/ℓ_g would appear in equation (31). Not accounting
 377 for this parameter effectively leaves a grid cell size dependence in the nondimensional-
 378 ization, which is something we seek to avoid.

379 Next we relax our constraint of $Q^* = 1$ and incorporate the hydrology equations
 380 into the scaling analysis. This model is called *DupuitLEM*. Because the hydrological model
 381 is linked to the geomorphic model through the dimensionless variable Q^* , the set of trans-
 382 formations used for the geomorphic equations above is not necessarily applicable to the
 383 *DupuitLEM* model. In addition to the characteristic scales used for the *NoHyd* model,
 384 ℓ_g , h_g , and t_g , we will introduce three scales particularly relevant to the hydrological pro-
 385 cesses: a characteristic aquifer thickness h_c , a characteristic aquifer drainage time t_d , and
 386 the recharge rate p . A simple mass balance of water in a 1D hillslope with length ℓ_g , re-
 387 lief h_g , recharge rate p , and hydraulic conductivity k_s gives:

$$p\ell_g = h_c k_s h_g / \ell_g,
 \tag{32}$$

388 while the characteristic drainage time can be derived for a shallow aquifer can be derived
 389 from C. Harman and Sivapalan (2009, their eq. 6), which likewise describes the drainage
 390 of an aquifer with characteristic length and relief with drainable porosity n :

$$t_d = \frac{\ell_g n}{k_s \sin \theta}
 \tag{33}$$

391 Making the approximation $\sin(\theta) \sim h_g/\ell_g$, the resulting characteristic scales are:

$$h_c = \frac{p\ell_g}{k_s h_g / \ell_g}
 \tag{34}$$

$$t_d = \frac{\ell_g n}{k_s h_g / \ell_g}
 \tag{35}$$

$$p
 \tag{36}$$

In addition to the recast landscape evolution equations in (20) and (21), we add those of the hydrological model:

$$\frac{\partial h}{\partial t} = \frac{h_c}{t_d} \left(1 - \frac{\nabla \cdot q}{p} - \frac{q_s}{p} \right) \quad (37)$$

$$\frac{q}{p} = -h \cos^2(\arctan |\nabla z|) \frac{\ell_g^2}{h_g h_c} (\nabla h + \nabla z) \quad (38)$$

$$\frac{q_s}{p} = \mathcal{G} \left(\frac{h}{b} \right) \mathcal{R} \left(1 - \frac{\nabla \cdot q}{p} \right) \quad (39)$$

$$Q^* = \frac{1}{Ap} \int_A q_s dA_c \quad (40)$$

392 Here we have expanded the aquifer base angle θ as $\arctan |\nabla z|$, as constant per-
 393 meable thickness implies that the aquifer base gradient is equal to the topographic gra-
 394 dient. As with the scaling analysis in equations (20) and (21), we can look for transfor-
 395 mations under which the equations are invariant. While the scaling in the time dimen-
 396 sion shown in (28) will apply as before, unlike in the geomorphic governing equations
 397 we cannot separately transform the vertical and horizontal length scales in the hydro-
 398 logic equations. The aquifer specific discharge q cannot be separated from the topographic
 399 gradient ∇z due to the cosine term in (38). As a result, there are only two transforma-
 400 tions that produce invariance:

$$\begin{aligned} & \{t \rightarrow ct, t_g \rightarrow ct_g, t_d \rightarrow ct_d\} \\ & \{x \rightarrow cx, y \rightarrow cy, a \rightarrow ca, A \rightarrow c^2 A, l_g \rightarrow cl_g, \\ & \quad q \rightarrow cq, z \rightarrow cz, h \rightarrow ch, h_g \rightarrow ch_g, h_c \rightarrow ch_c, b \rightarrow cb\} \end{aligned} \quad (41)$$

401 Again, we can choose scales c and apply the transformations in search of a form
 402 that eliminates or consolidates the characteristic scales. We will first apply the time trans-
 403 formation, choosing $c = 1/(t_g t_d)$. This is equivalent to applying the transformation twice,
 404 once with $c = 1/t_g$ and again with $c = 1/t_d$. We will then apply the second transfor-
 405 mation, choosing $c = 1/(\ell_g h_g h_c)$. Likewise, this is equivalent to applying the transfor-
 406 mation three times with each of the three factors in the denominator. In addition to the
 407 rescaled variables presented in (29), we add several additional rescaled variables:

$$\begin{aligned} h &= h' h_c \\ t &= t' t_d \\ q &= q' p \ell_g \\ q_s &= q'_s p \end{aligned} \quad (42)$$

Applying the two transformations, and employing the above definitions, we find find the governing equations simplify to the following:

$$\frac{\partial z'}{\partial t'} = -Q^* \sqrt{a'} |\nabla' z'| + \nabla'^2 z' + 1 \quad (43)$$

$$-\nabla' \cdot \left(a' \frac{\nabla' z'}{|\nabla' z'|} \right) = 1 \quad (44)$$

$$\frac{\partial h'}{\partial t} \frac{t_d}{t_g} = 1 - \nabla' \cdot q' - q'_s \quad (45)$$

$$q' = -h' \cos^2(\arctan |\nabla' z' h_g / \ell_g|) \left(\nabla' h' \frac{h_c}{h_g} + \nabla' z' \right) \quad (46)$$

$$= -h' \frac{\nabla' h' h_c / h_g + \nabla' z'}{1 + (h_g / \ell_g)^2 |\nabla' z'|^2} \quad (47)$$

$$q'_s = \mathcal{G} \left(h' \frac{h_c}{b} \right) \mathcal{R} \left(1 - \nabla' \cdot q' \right) \quad (48)$$

$$Q^* = \frac{1}{A'} \int_{A'} q'_s dA' \quad (49)$$

408 Our use of Q^* as a dimensionless representation of hydrology in the geomorphic
 409 equation means that we are still able to obtain a parameterless expression for topographic
 410 evolution, even though we have not separated the transformation of vertical and hori-
 411 zontal length scales in the hydrologic governing equations. There are, however, four pa-
 412 rameter groups that we cannot eliminate. We will give them the following names, which
 413 will be used throughout the rest of this paper:

$$\delta = \frac{t_d}{t_g} = \frac{n v_0^{2/3} D^{2/3} K^{4/3}}{k_s U} \quad (50)$$

$$\alpha = \frac{h_g}{\ell_g} = \frac{U}{v_0^{1/3} D^{1/3} K^{2/3}} \quad (51)$$

$$\gamma = \frac{b}{h_c} = \frac{b k_s h_g}{p \ell_g^2} = \frac{b k_s U}{p D} \quad (52)$$

$$\text{Hi} = \frac{h_g}{h_c} = \frac{k_s h_g^2}{p \ell_g^2} = \frac{k_s U^2}{p v_0^{2/3} D^{2/3} K^{4/3}} \quad (53)$$

414 Here δ represents the scaling between the hydrologic and geomorphic timescales
 415 of the model. By the nature of hydrologic and geomorphic processes, we expect this ratio
 416 to be very small in all cases. Additionally, δ multiplies the time rate of change of aquifer
 417 thickness, which should also be very small here as we only consider steady recharge. α
 418 is a characteristic gradient of the model that emerges from the geomorphic parameters.
 419 We will call γ the drainage capacity, as it is proportional to the maximum transmissiv-
 420 ity and the characteristic topographic gradient and inversely proportional to the mean
 421 recharge rate. Hi is analogous to the Hillslope number Hi presented by Brutsaert (2005)
 422 (Eq. 10.139) and used by C. Harman and Sivapalan (2009), C. J. Harman and Kim (2019),
 423 and others to understand shallow groundwater dynamics. It represents the relative im-
 424 portance of topographic gradients, versus diffusion of the water table, in driving ground-
 425 water flow. It can be thought of as a Peclet number, as it captures the ratio of advective
 426 to diffusive processes.

427

4.1 Special cases

428

429

430

431

432

433

434

These equations and parameters all apply in the general case when aquifer and topographic gradients are important drivers of groundwater flow. The expressions can be simplified under conditions where one gradient is more important than the other, reducing the constraints on our symmetry groups. Suppose that relief is generally large in comparison to aquifer thickness, $h_g \gg h_c$, in which case $Hi \gg 1$. Consequently, topographic gradients rather than aquifer thickness gradients tend to drive groundwater flow. In this case we neglect ∇h , altering the groundwater specific discharge expression (38):

$$\frac{q}{p} = -h \cos^2(\arctan |\nabla z|) \frac{\ell_g^2}{h_g h_c} \nabla z \quad (54)$$

435

436

437

438

Applying our symmetry method as before, we find that ℓ_g and h_g must still be scaled together. However, this time, h need not be scaled with these simultaneously in order to obtain a consistent set of equations. Instead, there are now three transformations that comprise the symmetry:

$$\begin{aligned} &\{t \rightarrow ct, t_g \rightarrow ct_g, t_d \rightarrow ct_d\} \\ &\{h \rightarrow ch, h_c \rightarrow ch_c, b \rightarrow cb\} \\ &\{x \rightarrow cx, y \rightarrow cy, a \rightarrow ca, A \rightarrow c^2 A, l_g \rightarrow cl_g, \\ &\quad q \rightarrow cq, z \rightarrow cz, h_g \rightarrow ch_g\} \end{aligned} \quad (55)$$

439

440

441

Implementing the three transformations above with $c = 1/t_g$, $c = 1/h_c$, and $c = 1/(h_g \ell_g)$ respectively, we arrive at a rescaled set of governing equations similar to previous, only with an altered expression for q' :

$$q' = -h' \cos^2(\arctan |\nabla' z' h_g / \ell_g|) \nabla' z' \quad (56)$$

442

443

444

445

446

Here the factor $Hi = h_g/h_c$ no longer appears in the equation. This suggests that the solution to the full governing equations should be independent of Hi when Hi is large. This makes sense in the context of Equation (47), as $1/Hi$ multiplies the gradient in aquifer thickness, which by definition will be small relative to topographic gradients when Hi is large.

447

448

449

450

451

Conversely, suppose that topographic gradients were largely insignificant, and flow was generally driven by gradients in aquifer thickness ($\nabla h \gg \nabla z$). In this case, the expression for groundwater specific discharge changes again, as we can approximate $\cos \theta \approx 1$ and $\nabla z \approx 0$ for the purposes of groundwater flow. Then the governing equations are again the same except for q :

$$\frac{q}{p} = -h \frac{\ell_g^2}{h_g h_c} \nabla h \quad (57)$$

452

453

454

455

456

In this case, because the cosine term does not appear, ℓ_g and h_g need not be scaled together. As in the previous case, there are three transformations that maintain symmetry, with a separate scaling for aquifer thickness h . However, in order to maintain consistency in the groundwater specific discharge equation, the vertical coordinate and h_g must be scaled with h .

$$\begin{aligned} & \{t \rightarrow ct, t_g \rightarrow ct_g, t_d \rightarrow ct_d\} \\ & \{h \rightarrow ch, h_c \rightarrow ch_c, b \rightarrow cb, z \rightarrow cz, h_g \rightarrow ch_g\} \\ & \{x \rightarrow cx, y \rightarrow cy, a \rightarrow ca, A \rightarrow c^2A, l_g \rightarrow cl_g, q \rightarrow cq\} \end{aligned} \quad (58)$$

457 Noting that these transformations are simply a rearrangement of the previous, we
 458 select the scales $c = 1/t_g$, $c = 1/(h_c h_g)$, and $c = 1/\ell_g$ respectively. We arrive at a
 459 rescaled set of governing equations when flow is primarily driven by gradients in aquifer
 460 thickness. Only the expression for q' has changed:

$$q' = -h' \frac{\nabla' h'}{\text{Hi}} \quad (59)$$

461 Under these conditions, the factor $\text{Hi} = h_g/h_c$ still appears in the groundwater
 462 specific discharge expression, while the parameter $\alpha = h_g/\ell_g$ no longer appears. This
 463 suggests that as Hi becomes small, the sensitivity to Hi does not decrease, but sensitiv-
 464 ity to α does decrease. Small Hi indicates that water table gradients are more impor-
 465 tant than topographic gradients in driving flow. As α is a measure of topographic gra-
 466 dients, it is appropriate that it should diminish in importance when Hi is small. The two
 467 end-member scenarios, where hydraulic gradients are alternately driven by topography
 468 or aquifer thickness, provide insight into expected parameter sensitivity, which we will
 469 test with the numerical model. In particular, we expect that for low values of Hi , the so-
 470 lution should be generally insensitive to the value of α , while the sensitivity to Hi will
 471 be small for high values of Hi . Overall, we have reduced the governing equations from
 472 a system with 7 parameters to a system with 4 parameters, one of which we expect one
 473 to be unimportant in all cases (δ). This significantly improved our ability to explore and
 474 comprehend the parameter space in the following sections.

475 5 Results

476 We explore the properties of the scaled model through a series of simulations de-
 477 signed to sample the nondimensional parameter space of α , γ , and Hi . While the fourth
 478 dimensionless parameter, δ , does vary as we vary hydrological parameters, this effect should
 479 be negligible for reasons previously stated.

480 We consider two cases of simulations. First, simulations with the *NoHyd* model in
 481 which $Q^* = 1$ and second, simulations with *DupuitLEM* in which Q^* varies in space
 482 and time. Such variation may arise under steady, uniform recharge as shallow subsur-
 483 face aquifer does not uniformly exfiltrate. Here time variation of Q^* is only due to changes
 484 in geomorphic boundary conditions. Additional complexity could be added by consid-
 485 ering time and/or spatially varying recharge—we do not consider this here. We evalu-
 486 ated the condition of steady state topography on the basis of change in mean dimension-
 487 less relief R_h/h_g , where R_h is the mean value of elevation z . For runs of the *NoHyd* model
 488 and runs of the *DupuitLEM* model where $\gamma < 1$, the results show clear indications of
 489 steady state, as the absolute value of dimensionless rate of relief change $|\frac{dR_h/h_g}{dt/t_g}|$ declines
 490 below 10^{-10} . In cases with larger γ , perturbations continue through time in the abso-
 491 lute value of relief change. We run the model at least until there is no decreasing trend
 492 in the absolute value of relief change. Times to meet these conditions range from approx-
 493 imately 300-2000 t_g , around 7-45 million years.

494 5.1 Confirmation of scaling and similarity

495 The numerical results confirm the scaling predicted in our similarity analysis. In
 496 Figure 1A (i, ii, iii) we show that ℓ_g can be varied independently from h_g (changing α)

497 with the *NoHyd* model and we can still obtain visually and numerically identical results
 498 in the rescaled coordinate system (x', y', z') . The same similarity appears when h_g is var-
 499 ied independently while ℓ_g remains constant (i, iv, vi) and when h_g and ℓ_g are varied to-
 500 gether (i, v, vii). The mean absolute difference in z' between all model runs is less than
 501 $10^{-13}\%$ of total relief. These results confirm the scaling found by Theodoratos et al. (2018),
 502 showing that the vertical and horizontal dimensions possess distinct and independent
 503 scaling relationships. Our similarity approach also predicts that the vertical and hori-
 504 zontal length scales should not scale independently in the *DupuitLEM* model, unless $Hi \ll$
 505 1. Figure 1B shows the same scaling of h_g and ℓ_g implemented in Figure 1A, now us-
 506 ing the *DupuitLEM* model with $Hi = 5$ and $\gamma = 2.5$. As ℓ_g is increased independent
 507 of h_g (i, ii, iii), α decreases and the distance between channels appears to increase. Sim-
 508 ilarly as we increase h_g while holding ℓ_g constant (i, iv, vi), α increases and we observe
 509 a decrease in spacing between channels. It is only when h_g and ℓ_g are varied together
 510 (i, v, vii), keeping α constant, that topography remains invariant in the rescaled coor-
 511 dinates. There is less than 2% difference in mean relief between the results in (i, v, vii).
 512 While sufficient to confirm the scaling analysis, this difference is larger to that observed
 513 in 1A due to isolated areas that develop slightly different drainage patterns. This is likely
 514 as a result of small numerical differences between the groundwater model solutions early
 515 in the evolution of topography.

516 Our similarity analysis suggested that vertical and horizontal dimensions should
 517 scale independently when Hi is small. In this case, relief is small relative to the charac-
 518 teristic aquifer thickness, and as a result it should not play a strong role in generating
 519 hydraulic gradients that drive flow. Figure 1C shows the results of the same variation
 520 in h_g and ℓ_g as Figure 1B, but now with $Hi = 0.01$. In this case, h_g and ℓ_g appear to
 521 scale independently for relatively small values of α (< 0.2). Plots (i, iv, vi) do still show
 522 some topographic variation between model runs, while (i, ii, iii) do not. While this pro-
 523 vides some confirmation of our scaling analysis, in the cases we will test going forward,
 524 Hi values will generally not be small enough for the results to be independent of α .

525 5.2 Sensitivity to dimensionless hydrologic parameters

526 The results suggest that landscape and climate properties affecting shallow ground-
 527 water flow could have major effects on topography. There are strong differences in to-
 528 pography between model runs when dimensionless parameters describing these factors
 529 are varied. In particular, the evolved topography is strongly dependent on the drainage
 530 capacity γ , which is the ratio of soil depth b to characteristic aquifer thickness $h_c = \frac{D\ell_g^2}{k_s h_g}$.
 531 When $\gamma = 0.5$, the lowest value shown in Figure 2, the results look very similar to those
 532 obtained with the *NoHyd* model. In these cases the entire landscape experiences some
 533 overland flow and erosion, which is apparent in the spatial distribution of Q^* shown in
 534 Figure 4. In contrast, high γ cases produce broad interfluves where $Q^* = 0$, as the wa-
 535 ter table sits further below the surface. As a result these areas do not experience sur-
 536 face erosion. To a lesser degree, Hi affects the steady state topography as well. As dis-
 537 cussed previously, Hi describes the characteristic relief relative to the characteristic aquifer
 538 thickness. From the the hillshades presented in Figure 2, it appears that Hi has the great-
 539 est influence on topography when drainage capacity γ is large, in which case increasing
 540 Hi generally decreases the spacing between channels. The previous section evaluating
 541 the scaling properties of the model results showed that α has a significant effect on to-
 542 pography in most cases where Hi is not very small. The supplemental material includes
 543 figures showing the results of varying γ and Hi with higher and lower values of α than
 544 those shown here. While transitions in morphology and runoff happen at different val-
 545 ues of γ and Hi when α is varied, the fundamental dependence on these parameters re-
 546 mains the same.

547 Distributions of Q^* represent the spatial variability in runoff that emerges from our
 548 coupled geomorphic-hydrologic model under conditions of steady, uniform recharge. These

distributions confirm that the extent of areas contributing runoff tends to decrease with increasing γ , and to a lesser extent with decreasing H_i . Figure 4B shows cumulative distribution functions of Q^* for each model run, indicating the proportion of the landscape where Q^* is less than a particular value on the x-axis. Strikingly, we see that areas that contribute no runoff ($Q^* = 0$) first appear exactly when $\gamma = 1$ (third row from the bottom). This holds for smaller and larger values of α as well (see Figures S3, S6). It is at this point that the spatial variability in Q^* is maximized: at lower values all areas contribute some runoff, while above this value, most areas contribute no runoff at all. As γ is the ratio of the characteristic aquifer thickness h_c to the permeable thickness b , a value of 1 should indicate that a “characteristic hillslope” has just become saturated, which appears to be in agreement with our results. This is a powerful demonstration of the effectiveness of this nondimensionalization.

In Figure 4C, the proportion of computational grid nodes with $Q^* > 0.5$ indicates extensive saturation in low γ cases with minor sensitivity H_i values; the extent of runoff contributing areas declines slightly more rapidly when H_i is large. For comparison, we also plot the proportion of the landscape with positive curvature, which shows a more gradual change with γ .

Clearly subsurface hydrology is having a strong effect on topography in this model. With increasing ability to drain water through the subsurface (large γ), less surface drainage is needed, and consequently, the spacing between streams is greater. Furthermore, landscapes with lower drainage capacity (smaller γ) have larger source areas of overland flow extending across more the landscape. When drainage capacity is larger, the landscape is generally steeper and saturated areas are restricted to narrow incised regions. The patterns of Q^* indicate that $\gamma = 1$ defines the transition between landscapes that evolve with these two behaviors.

6 Emergent properties at landscape equilibrium

6.1 Topographic analysis: steepness and curvature

The landscapes shown in Figures 1, 2 and 4 reveal the visually striking influence of hydrological properties on landscape form. However, there is still much more we can learn about the controls on these emergent properties, guided by the form of the governing equations. Furthermore, we would like to be able to develop some quantitative understanding that relates readily observable topographic features to hydrological properties that are more difficult to measure. The relationships between model parameters and emergent hydrologic and geomorphic properties will be the focus of this section.

Commonly, properties of stream channels and entire landscapes are examined by plotting local slope versus accumulated area (e.g., Tarboton et al., 1989; Willgoose, Bras, & Rodriguez-Iturbe, 1991; Dietrich et al., 1993). Results form point clouds where zones of distinct behavior can be identified (Perron et al., 2008). Recently, Theodoratos et al. (2018) showed that the topography resulting from the streampower-linear diffusion LEM may be analyzed by examining relationships between what they term the incision height $\sqrt{A}|\nabla z|$ and Laplacian curvature $\nabla^2 z$. (Theodoratos & Kirchner, 2020b) refer to $\sqrt{A}|\nabla z|$ as steepness, so here we will adopt similar terminology, with one difference: to match the form of our governing equations, we define steepness as $\sqrt{a}|\nabla z|$, using area per contour width a rather than area A . Steepness and curvature emerge naturally from the steady state form of the governing equation for topographic evolution (20). Setting the time rate of change equal to zero, and rearranging, we obtain the following relationship:

$$\nabla^2 z = \ell_g^{-3/2} Q^* \sqrt{a} |\nabla z| - \frac{h_g}{\ell_g^2} \quad (60)$$

which has the equivalent dimensionless form:

$$\nabla'^2 z' = Q^* \sqrt{a'} |\nabla' z'| - 1 \quad (61)$$

595 When runoff generation is spatially uniform and therefore $Q^* = 1$ for all (x, y) ,
 596 as in the *NoHyd* model, there is a linear relationship between steepness and curvature,
 597 with a slope of unity and intercept of -1 in dimensionless coordinates, as observed by Theodoratos
 598 et al. (2018). While this definition of steepness is contingent on the particular exponents
 599 on area and slope, Theodoratos et al. (2018) showed that this relationship can be gen-
 600 eralized to any exponent values, albeit with significantly more complicated formulas.

601 Figure 5 shows topography from a run of the *NoHyd* model in slope-area and steepness-
 602 curvature space. The results show the expected slope and intercept in the steepness-curvature
 603 plot. All of the variability that appears in the slope-area space collapses onto a single
 604 line in steepness-curvature space, making steepness-curvature plots powerful tools for ex-
 605 amining model behavior. Observing this relationship in the numerical solution also demon-
 606 strates that the model accurately reproduces the analytical result at steady state.

607 Furthermore, deviations created by the introduction of hydrologic variability with
 608 Q^* should be readily apparent when plotting steepness versus curvature. When we use
 609 the *DupuitLEM* model, plotting $Q^* \sqrt{a'} |\nabla' z'|$ rather than $\sqrt{a'} |\nabla' z'|$ versus curvature would
 610 again result in a linear relationship. Through topographic analysis alone, however, steep-
 611 ness and curvature are available while Q^* is not. Quantifying the relationship between
 612 these topographically-derived quantities and Q^* across each steady state landscape in
 613 our nondimensional parameter space thus supports quantifying hydrological function based
 614 upon topography.

615 Slope-area and steepness-curvature plots for selected model runs with different val-
 616 ues of γ and H_i are shown in Figure 6. The steepness-curvature relationships for the low
 617 γ cases show close agreement with the theoretical relationships derived from the *NoHyd*
 618 model (dotted black line). This is consistent with the observed values of Q^* , which are
 619 close to unity at most nodes. With increasing drainage capacity γ , there is an apparent
 620 separation between points that conform to the theoretical relationship and points that
 621 maintain constant negative curvature $\nabla^2 z = -h_g/\ell_g^2$. The difference between these be-
 622 haviors is revealed in the values of Q^* . Areas in yellow have $Q^* \approx 0$, and form the zone
 623 of constant negative curvature. This is exactly what we would expect from the solution
 624 to the steady state equation (61) in the absence of the fluvial incision term. Points in
 625 this zone are divergent hillslopes that do not reach surface saturation. Areas in blue have
 626 $Q^* \approx 1$, essentially conforming to the same relationship observed for the *NoHyd* model.
 627 Points in this zone are the fluvial valleys that are fully saturated and have discharge ap-
 628 proximately equal to upslope area times the recharge rate. This indicates that at these
 629 locations the vast majority of water is moving over the surface rather than through the
 630 subsurface. A limited number of points fall in between these two end members of behav-
 631 ior. These are the channel heads and other areas of limited runoff contribution, where
 632 $0 < Q^* < 1$. When $\gamma > 1$, the proportion of points in this intermediate space ap-
 633 pears to decrease with increasing γ .

634 Slope-area plots do show separation between these behaviors, though the end mem-
 635 bers of behavior are not nearly as distinct. Differences between channel and hillslope mor-
 636 phology are also apparent in map view plots of steepness and curvature (Figure 7). While
 637 steepness does seem to provide an indication of increasing channelization in the low γ
 638 cases, in the high γ cases, it takes on unusual swirling patterns on hillslopes, in part due
 639 to the D8 flow routing method. These are of little consequence in the context of processes
 640 acting in the model, because on these hillslopes $Q^* \rightarrow 0$ and therefore the fluvial in-
 641 cision term that also goes to zero. Map view curvature plots show that in low γ cases,
 642 areas of negative curvature are restricted to narrow areas near the ridges, while exten-

sive areas have near zero or positive curvatures, indicating predominantly concave-upward terrain. In comparison, in high γ cases, most points obtain a constant negative curvature, representing convex-upward hillslopes, while the channels obtain large positive curvatures as a consequence of the steep adjacent hillslopes.

6.2 Hydromorphic balance

How can we understand the separation between channel and hillslope behavior that appears in the *DupuitLEM* model results? While there is a unique relationship between steepness and curvature for the *NoHyd* model, this is no longer the case for the *DupuitLEM* model, indicating that some information is not captured by these terms alone. The missing piece, as equation (61) shows, is Q^* . That is, there is a unique relationship between steepness, curvature, and Q^* . If we would like to know Q^* , one approach would be to solve for Q^* and explore how it could be determined from the governing equations. Using the equation for topography at steady state (20), we find Q^* as a function of the parameters, steepness, and curvature.

$$Q^* = \ell_g^{3/2} \frac{\nabla^2 z}{\sqrt{a}|\nabla z|} + \frac{h_g}{\sqrt{\ell_g}} \frac{1}{\sqrt{a}|\nabla z|} \quad (62)$$

We will call this equation the *Geomorphic Balance*. Results of plotting Q^* versus the right hand side of this equation are shown in Figure 9A. Like the relationship between steepness and curvature for the *NoHyd* model, the geomorphic balance shows a tight linear relationship. In other words, most places in the landscape have topography that is closely coupled with the runoff at that location, as predicted by the governing equations. Deviation from the 1:1 line in Figure 9A is an indication that the hydrologic state and geomorphic state are not completely in equilibrium with one another. These deviations likely have a similar origin to the perturbations in relief as the model evolves toward topographic steady state that we noted previously. Both indicate that subtle adjustments between the hydrologic and geomorphic states persist in the evolution of the modeled landscapes. This demonstration of dynamic equilibrium has similarities to natural settings where adjustment to small perturbations is persistent even in landscapes that are considered to be near geomorphic steady state.

Unfortunately in most cases where one might want to apply the *Geomorphic Balance* to real data to determine spatial patterns of runoff and saturation, the geomorphic length scales h_g and ℓ_g are unknown. While the *NoHyd* model has distinct relationships between landscape properties and h_g and ℓ_g , explored by Theodoratos et al. (2018), those relationships break down with the addition of subsurface hydrology. Even if we were to estimate h_g and ℓ_g through geomorphic methods, the uncertainty in direct estimates these parameters is likely far too great to constrain Q^* in (62).

However, the hydrologic equations offer a complementary solution for Q^* . At hydrological steady state, for steady recharge at rate p , the expression for conservation of mass (16) can be written as:

$$p = \nabla \cdot q + q_s \quad (63)$$

This should be a reasonable representation of our results, as the recharge rate is constant, and other properties vary slowly with time. Integrating this water balance over the watershed area, A , and using Leibniz' rule to evaluate the integral of the divergence term:

$$\int_A p dA = \int_A (\nabla \cdot q + q_s) dA \quad (64)$$

$$pA = \iint \nabla \cdot q dx dy + Q^* pA \quad (65)$$

$$pA = \oint_c q \cdot n dS + Q^* pA \quad (66)$$

683 If we assume that the catchment boundary is a no-flux boundary except for the out-
 684 let with characteristic contour width v_0 , then this reduces to:

$$pA = qv_0 + Q^* pA \quad (67)$$

685 This also assumes that groundwater flux is directed out of the watershed, which
 686 is a tenuous assumption for deeper regional aquifers but perhaps is appropriate for the
 687 shallow near-surface aquifers that tend to produce return flow and near-channel areas
 688 of surface saturation during rainfall events. We selected the characteristic contour width
 689 v_0 here to be the same as the contour width used in (8), so the relationship $A = v_0 a$
 690 still holds. Next we substitute the expression for groundwater flow (17). Assuming gra-
 691 dients are directed out of the watershed, we can take the absolute value of gradients for
 692 similarity to the geomorphic balance.

$$pA = v_0 k_s h (|\nabla h| + |\nabla z|) \cos^2(\theta) + Q^* pA \quad (68)$$

then substituting $A = av_0$ and rearranging to solve for Q^* :

$$Q^* = 1 - \frac{k_s h (|\nabla h| + |\nabla z|) \cos^2(\theta)}{p a} \quad (69)$$

693 By limiting ourselves to locations where the water table has reached the land sur-
 694 face so that the aquifer base and land surface are parallel, we can set $h \rightarrow b$ and $\nabla h \rightarrow$
 695 0.

$$Q^* = 1 - \frac{k_s b |\nabla z| \cos^2(\theta)}{p a} \quad (70)$$

696 This is our *Hydrologic Balance* expression for Q^* . Contained in this expression is
 697 a modified version of the topographic index $\frac{a}{\nabla z \cos^2(\theta)}$, where we have retained the co-
 698 sine term for similarity to the governing equation for groundwater flow. It is appropri-
 699 ate that topographic index should appear in this equation, as it has been shown to be
 700 a useful tool for understanding geomorphically-driven hydrological behavior (Beven &
 701 Kirkby, 1979). The results of plotting Q^* against the right hand side of (70) are shown
 702 in Figure 9B. Correlations are not as strong as geomorphic balance. One trend that emerges
 703 is that at high drainage capacity (large γ), the fit to the theoretical curve improves as
 704 Hi increases. As discussed previously, when Hi is small, diffusive fluxes driven by gra-
 705 dients in aquifer thickness rather than topography are important for determining ground-
 706 water fluxes. This is something not captured in our simplified steady state model. Fur-
 707 ther investigation revealed that differences between modeled results and our analytical
 708 solution result from differences in methods of surface versus subsurface flow routing. Sub-
 709 surface flow is calculated in a “diffusive” sense by measuring fluxes in or out on all links
 710 connecting nodes of the computational mesh. In contrast, surface routing is calculated
 711 with an “advective”, steepest-descent approach, where all flow is routed downslope from
 712 one single node to another. The analytical solution assumes that the recharge on the up-

713 slope area, which we calculate with the “advective” method, is the total flow that is par-
 714 titioned between surface and subsurface flow at a node. This may not always be a good
 715 assumption. Numerous unsuccessful attempts to circumvent this problem suggest that
 716 this may in fact be an intrinsic feature of a model (and perhaps reality) in which sur-
 717 face flow is rapid and generally channelized in a single direction, while groundwater flow
 718 is more gradual and diffusive in nature. Even with these limitations, we can continue to-
 719 ward a result with the analytical solution we have presented.

720 Now we have two expressions for Q^* : one hydrologic in (70) and one geomorphic
 721 in (62). We can combine these expressions by eliminating Q^* and obtain:

$$1 - \frac{bk_s}{p} \frac{|\nabla z| \cos^2(\theta)}{a} = \ell_g^{3/2} \frac{\nabla^2 z}{\sqrt{a}|\nabla z|} + \frac{h_g}{\sqrt{\ell_g}} \frac{1}{\sqrt{a}|\nabla z|} \quad (71)$$

or equivalently:

$$0 = \frac{bk_s}{p} \left(\frac{|\nabla z| \cos^2(\theta)}{a} \right) + \ell_g^{3/2} \left(\frac{\nabla^2 z}{\sqrt{a}|\nabla z|} \right) + \frac{h_g}{\sqrt{\ell_g}} \left(\frac{1}{\sqrt{a}|\nabla z|} \right) - 1 \quad (72)$$

722 We call this expression the *Hydromorphic Balance*. It describes a fundamental re-
 723 lationship between steepness, curvature, and topographic index that emerges from the
 724 governing equations. This relationship suggests that values of the three terms in paren-
 725 thesis (which can all be calculated directly from a digital elevation model) should form
 726 a surface with linear coefficients bk_s/p , $\ell_g^{3/2}$, and $h_g/\sqrt{\ell_g}$ respectively. Using the same
 727 nondimensionalization as previously, (72) can be rewritten simply as:

$$0 = \frac{\gamma}{T_z} + \frac{C_z}{S_z} + \frac{1}{S_z} - 1 \quad (73)$$

728 where $T_z = \frac{\nabla'z' \cos^2(\theta)}{a'}$ is the dimensionless topographic index, $S_z = \sqrt{a'}|\nabla'z'|$
 729 is the dimensionless steepness, and $C_z = \nabla'^2z'$ is the dimensionless curvature. We do
 730 not expect points where $Q^* = 0$ to conform to this relationship—such as where the wa-
 731 ter table does not reach the surface—because the hydrologic component of this balance
 732 is no longer valid. An alternative way to view the components of the *Hydromorphic Bal-*
 733 *ance* is in map view, separating out the terms and examining their spatial patterns. Fig-
 734 ure 10 shows the terms of (73) for four different parameter combinations (the four cor-
 735 ners of the space plotted in Figures 9A and 9B). The results show differing importance
 736 of terms in the low and high γ cases, with C_z/S_z more important when γ is large, and
 737 $1/S_z$ more important when γ is small. Large γ cases attain larger steepness and larger
 738 curvature than the low γ counterparts. Here we limit our scope to places where $Q^* >$
 739 0.001 . While in application, this kind of threshold would not be known, the relationship
 740 between Q^* and curvature (not shown) suggests that it would be sufficient to use the slightly
 741 more restrictive condition $\nabla^2 z > 0$ to determine areas of the landscape that should con-
 742 form to the *Hydromorphic Balance*.

743 6.3 Emergent hillslope length

744 The perception that emergent length scales of the ridge-valley topography increase
 745 with drainage capacity can be quantified by measuring and comparing the average hill-
 746 slope length L_h . Here, we define L_h as the mean distance from hillslope points to the
 747 nearest channel. This is inversely proportional to twice the drainage density, where drainage
 748 density is calculated with the method described by Tucker et al. (2001). Hillslope length
 749 is of particular interest in the context of hydraulic groundwater theory, where it is both
 750 an important control on hillslope storage and characteristic response time (C. Harman

751 & Sivapalan, 2009; Troch et al., 2003). A measure of hillslope length depends on the de-
 752 delineation of channel locations. While it is common to use threshold values of steepness
 753 index to identify channels (e.g., Tucker et al., 2001), this implicitly assumes a relation-
 754 ship between steepness and incision, which is not the case in the *DupuitLEM* model. In-
 755 stead, we identify channels as points of positive Laplacian curvature ($\nabla^2 z > 0$), where
 756 fluvial incision is the dominant geomorphic process.

757 We can use the hydromorphic balance to predict the scaling relationship between
 758 hillslope length and the drainage capacity γ . We begin with the hydrologic and geomor-
 759 phic balance expressions, equations (70) and (62). This time, rather than combining to
 760 eliminate Q^* as we did previously, we can combine to eliminate the topographic gradi-
 761 ent $|\nabla z|$. Since we have defined channels as places where $\nabla^2 z > 0$, channel heads can
 762 be defined as places where $\nabla^2 z = 0$. We can apply the latter condition to the geomor-
 763 phic balance to obtain an expression for the critical upslope area per contour width a_c
 764 at channel heads. We cannot eliminate all instances of the gradient in the hydromorphic
 765 balance, as it is present in the term $\cos(\theta) = \cos(\arctan |\nabla' z' h_g / \ell_g|)$. Here we will make
 766 the assumption that the dimensionless gradient in this term is equal to one at channel
 767 heads, such that $\cos(\theta) \approx \cos(\arctan(\alpha))$. Assuming θ is similar at channel heads across
 768 our parameter space, this assumption should only affect the coefficient scaling γ and hill-
 769 slope length. We must also choose a value for Q^* in order to find a solution for both the
 770 *Hydrologic balance* and *Geomorphic Balance*, as we have not eliminated it in this case.
 771 Our results show that Q^* can vary substantially at locations of zero Laplacian curva-
 772 ture (not shown), but here we will introduce a constant characteristic value Q_c^* for the
 773 purposes of finding a solution. Applying these conditions, we find that the hydromor-
 774 phic balance gives an expression for the area per contour width at channel heads a_c :

$$\frac{a_c}{l_g} = \left(\frac{\gamma / Q_c^{*2}}{1 + \alpha^2} \right)^{2/3} \quad (74)$$

$$= \left(\frac{bk_s}{pQ_c^{*2}} \frac{h_g}{h_g^2 + l_g^2} \right)^{2/3} \quad (75)$$

775 or, expanding out the definitions of h_g and l_g , we can solve for the critical area at
 776 channel heads, $A_c = a_c v_0$:

$$A_c = \left(\frac{v_0 bk_s}{pQ_c^{*2}} \hat{h}_g \right)^{2/3} \quad (76)$$

777 where \hat{h}_g is the inverse sum of two vertical length scales defined by the geomorphic
 778 variables:

$$\frac{1}{\hat{h}_g} = \frac{K}{U} + \frac{U}{\sqrt[3]{D^2 K v_0^2}} \quad (77)$$

779 The scaling confirms our previous observations that increasing the drainage capaci-
 780 ty γ leads to greater spacing between channels, and therefore larger source areas at chan-
 781 nel heads. Intuitively, this suggests that the landscape is less dissected when more flow
 782 drains through the subsurface. The expanded relationship shows a similar story: increas-
 783 ing $v_0 bk_s$ leads to larger contributing areas at channel heads, while increasing recharge
 784 rate p or effectiveness of fluvial incision relative to uplift lead to smaller contributing ar-

785 eas at channel heads. From here we further assume that the hillslope length at channel
 786 heads is proportional to the area per contour width, and thus $L_h/\ell_g \sim \gamma^{2/3}$. Despite
 787 the crudeness of this estimate, Figure 11 (left panel) shows that this scaling is in agree-
 788 ment with the model results when $\gamma > 1$.

789 7 Discussion

790 7.1 Hydrogeomorphic coevolution

791 The results presented here constitute one possible way that landscape history can
 792 be used to understand current hydrological processes by quantifying the coevolution of
 793 hydrological processes with landscape form (C. Harman & Troch, 2014; Troch et al., 2015).
 794 Prior attempts to use coevolution to understand hydrological flow paths and processes
 795 focus on evolving subsurface properties. Jefferson et al. (2010) and Yoshida and Troch
 796 (2016) explore how flow paths evolve on basaltic terrains, where porous young basalt ter-
 797 rains tend to drain flow vertically, while chemical weathering of basalt tends to progres-
 798 sively block flow paths with clays, leading to increased prevalence of lateral flow on older
 799 terrains. Both studies use space-for-time substitution to explore temporal changes in drainage
 800 density, but find contradictory trends, suggesting that underlying processes of drainage
 801 and erosion are still not well enough understood in these landscapes. Recent work on
 802 coevolution in denudational landscapes has focused on coevolution of subsurface flow paths
 803 and subsurface structure through the propagation of weathering fronts (Rempé & Di-
 804 etrich, 2014; C. J. Harman & Kim, 2019; C. J. Harman & Cosans, 2019; Brantley, Lebe-
 805 deva, et al., 2017). In these studies, continuous incision of streams is often used as a bound-
 806 ary condition to which hillslopes respond. In this study, we took a complementary ap-
 807 proach, enforcing constant regolith thickness and permeability, while exploring surface
 808 geomorphic evolution. We found that subsurface flow plays a critical role in setting hill-
 809 slope length, which may in turn affect the hydraulic gradients and flow rates that affect
 810 subsurface weathering processes. These results are consistent with the negative relation-
 811 ship between transmissivity and drainage density presented in Carlston (1963), and the
 812 inverse relationship between drainage density and hydraulic conductivity in the High Plains
 813 Aquifer measured by Luo and Pederson (2012). Approaches focused on surface and sub-
 814 surface may be unified to formulate more general theories of the evolution of denuda-
 815 tional landscapes.

816 7.2 Scaling and typology of landscapes

817 Our similarity approach expands upon the analysis of Theodoratos et al. (2018)
 818 and Bonetti et al. (2020). The analysis conducted by Theodoratos et al. (2018) showed
 819 that by selecting appropriate length and time scales, a standard form of the streampower-
 820 linear diffusion LEM—which uses A rather than a and does not consider an incision thresh-
 821 old or runoff coefficient—was parameterless, and thus had only a single landscape typology—
 822 assessed on the basis of topography—that could be rescaled to obtain every result the
 823 model could produce. As pointed out by Bonetti et al. (2020), the streampower-linear
 824 diffusion LEM does have an additional parameter, which is unaccounted for in Theodoratos
 825 et al. (2018) because the authors do not expose the differential equation that defines the
 826 upslope area per contour width. With this equation expressed, Bonetti et al. (2020) de-
 827 velop a nondimensionalization where one parameter remains, similar to the Peclet num-
 828 ber that appears in Perron et al. (2008). Our analysis of the streampower-linear diffu-
 829 sion LEM (called the *NoHyd* model here) shows that a parameterless set of equations
 830 can still be obtained from the governing equations when accounting for the upslope area
 831 differential equation. We show that, contrary to Bonetti et al. (2020), there is a single
 832 typology for the *NoHyd* model, which can be rescaled to obtain all results the model may
 833 produce.

834 We develop the scaling analysis further by including the effects of runoff generated
 835 from shallow unconfined groundwater flow. This introduces four dimensionless param-
 836 eters, of which three are important for the emergent topography. With this model, there
 837 is no longer a single landscape typology, but variation in form dependent on how flow
 838 is partitioned between surface and subsurface γ , the degree to which topography drives
 839 groundwater flow H_i , and the landscape gradient generated by underlying geomorphic
 840 processes α . Other typologies can certainly be imagined by the addition of other geo-
 841 morphic or hydrologic processes, including a channel incision threshold (Theodoratos &
 842 Kirchner, 2020a). However the one we present is unique in that it expresses feedbacks
 843 between hydrologic and geomorphic processes, which consequently link landscape typol-
 844 ogy to hydrologic function.

845 7.3 Characteristic contour width and valley transmissivity

846 We first introduced the concept of a characteristic contour width v_0 in order to write
 847 the channel scaling relationship (Equation 7) in terms of upslope area per contour width
 848 a rather than upslope area A . This proved useful in subsequent scaling analyses, where
 849 we developed a new parameterless scaling of the governing geomorphic equations that
 850 is only possible because we have accounted for v_0 in our definitions of the geomorphic
 851 length, height, and timescales ℓ_g , h_g , and t_g . We noted previously there that we are free
 852 to choose a value of v_0 , as there will always be a corresponding value of k_w to satisfy the
 853 relationship between w and a . What then is a physically meaningful characteristic con-
 854 tour width, and how would we identify it outside of the context of a landscape evolu-
 855 tion model? One possible explanation appears in the hydromorphic balance equation (76)
 856 for the upslope area at channel heads, A_c . Here the characteristic contour width appears
 857 in the numerator $v_0 b k_s$, which is effectively the transmissivity integrated across a char-
 858 acteristic contour width. This integrated transmissivity is particularly important at chan-
 859 nel heads, where relative magnitudes of surface and subsurface flow are similar. Upstream
 860 of the channel head, the contour width is less important, as topographic features do not
 861 constrict groundwater flow to a fixed width. Further downstream from the channel head,
 862 groundwater flow is constricted by the valley width, but most of the discharge will be
 863 transmitted as surface water rather than groundwater. Because A_c scales with v_0 just
 864 as it does with the transmissivity $b k_s$, v_0 plays a critical role in determining the extent
 865 of landscape dissection, as increasing channel head source areas increases the distance
 866 from channels to ridges. In landscapes similar to those modeled here, we suggest that
 867 the characteristic contour width is best thought of as characteristic channel head width,
 868 and that more attention should be paid to this factor in field investigations.

869 7.4 Landscape complexity

870 In developing this first systematic exploration of the effects of subsurface flow on
 871 steady state landscape form, we have neglected the complexity of landscape processes
 872 and heterogeneity of landscape properties in favor of an approach with a tractable num-
 873 ber of parameters so that we can explore the diversity of behaviors it can produce. How-
 874 ever, it is likely that processes and heterogeneity not captured here have significant im-
 875 pacts on landscape form. Subsurface properties are not only heterogeneous, but spatially
 876 organized, including systematic variations in permeability with depth through soil and
 877 weathered bedrock and along hillslope catenas (Lohse & Dietrich, 2005). The scope of
 878 runoff generation processes we have examined is also limited, as we have not considered
 879 infiltration excess overland flow, nor other erosional processes that are linked to shallow
 880 groundwater, including seepage erosion (Abrams et al., 2009; Laity & Malin, 1985) and
 881 landsliding driven by excess pore water pressure (Montgomery & Dietrich, 1994). Like-
 882 wise, ecological processes may act on the environment in ways that cannot be captured
 883 by the processes and parameters included here. For example, feedback between depth
 884 to water table and tree growth may affect spatial patterns of hillslope and fluvial sed-

885 iment transport, as trees anchor sediment with roots, displace sediment through treethrow,
886 or encourage soil production (Brantley, Eissenstat, et al., 2017; Gabet & Mudd, 2010).

887 7.5 Steady state topography

888 In this study we have focused on evaluating landscapes near topographic steady
889 state in order to understand the emergent relationships between topography and hydrology
890 generated by these governing equations. This is a powerful method employed in landscape
891 evolution models to understand the form toward which landscapes will evolve (e.g.,
892 Perron et al., 2008; Theodoratos et al., 2018). In the model we have used here, however,
893 times to steady state are long (millions to tens of millions of years) compared to real timescales
894 of variability in climate and baselevel change. For this reason, transience, at least in some
895 portions of the landscape, is likely the norm in real landscapes with similar dominant
896 processes to those modeled here (Whipple, 2001). On the other hand, nonlinear models
897 of hillslope diffusion show substantially shorter times to steady state (Roering et al.,
898 2001), which may be important when hillslopes are the limiting factor in reaching topographic
899 steady state. Further investigation could focus on transient responses the model
900 considered here, which may provide insights into a wider range of humid landscapes.

901 7.6 Steady recharge

902 In this model, we have shown that runoff generation from shallow groundwater driven
903 by steady recharge has a strong effect on emergent landscape properties. With increasing γ ,
904 we found that the hydrological function of the landscape was increasingly binary:
905 channels have surface runoff nearly equal to the sum of the recharge on the area upslope,
906 while hillslopes do not contribute surface runoff at all. While this may be characteristic
907 of some landscapes where saturated areas are more or less constant in time, in many
908 places, saturated areas and wetted channels expand and contract in response to the arrival
909 of storm events or snow melt (Dunne & Black, 1970; Nippgen et al., 2015; Antonelli
910 et al., 2020). Furthermore, antecedent wetness plays an important role in determining
911 the hydrological response to precipitation (Longobardi et al., 2003; O’Loughlin, 1981).
912 As fluvial sediment transport in our model is proportional to runoff Q^* , we expect that
913 precipitation stochasticity and subsurface water storage affect sediment transport and
914 thus ultimately will affect the landscape form as well. Previous studies have shown that
915 landscape form and channel profiles have are sensitive to variability in precipitation or
916 discharge, depending on factors including the presence of erosion thresholds and the non-
917 linearity of the fluvial incision model (Tucker, 2004; Lague et al., 2005; Deal et al., 2018).
918 In a future contribution, we will extend the theoretical framework used here to incor-
919 porate stochastic precipitation, allowing allowing us to explore the emergence of hydro-
920 geomorphic features such as variable source areas.

921 8 Conclusion

922 Here we have coupled a model of shallow groundwater flow with a model of denuda-
923 tional landscape evolution, and have shown the first results of such a model at topographic
924 steady state. The shallow aquifer model uses the Dupuit-Forcheimer assumptions to gener-
925 ate lateral groundwater flow and surface water discharge from groundwater return flow
926 and precipitation on saturated areas. The topography evolves according to fluvial inci-
927 sion by routed flow generated by the groundwater model, linear hillslope diffusion, and
928 a constant rate of uplift. We use a novel scaling analysis to guide or numerical simula-
929 tions, and find that the subsurface drainage capacity relative to climate plays a critical
930 role in setting topographic properties including hillslope length. We showed that the lin-
931 ear relationship between steepness and Laplacian curvature that emerges from the sim-
932 ple streampower incision-linear diffusion LEM bifurcates with increasing subsurface drainage
933 capacity: saturated areas tend toward the linear relationship between steepness and cur-

934 vature, while unsaturated hillslopes maintain constant negative curvature regardless of
935 steepness. By incorporating the steady state solution of the hydrological model, we can
936 explain the model results not as falling along a line of steepness and curvature, but as
937 sitting on a manifold that relates steepness, Laplacian curvature, and topographic in-
938 dex. A complementary analysis of the governing equations at steady state showed that
939 hillslope length should scale with the subsurface drainage capacity, and therefore the trans-
940 missivity, to the power $2/3$. This was supported by our numerical results for sufficiently
941 large drainage capacities. This analysis provides a pathway toward estimating subsur-
942 face transmissivity at the landscape scale using terrain analysis. Links between landscape
943 form and hydrologic function have been long sought-after in hydrology. Our work ex-
944 amines the possibility that an understanding of landscape history through the coevolu-
945 tion of landforms and hydrological process could be useful for generating hypotheses about
946 these relationships that can be tested against field data. If successful, this approach could
947 complement existing approaches for estimating hydrological parameters across regions
948 or continents that are often necessary to drive large scale hydrological and land surface
949 models.

950 **9 Notation**

951 Variable definitions are below, with dimensions length L, time T, and mass M. Prime
952 always indicates the dimensionless equivalent, where dimensionless equivalents are de-
953 fined in the text.

variable	name	dimension
x, y	horizontal coordinates	$[L]$
t	time	$[T]$
$z(x, y)$	topographic elevation	$[L]$
$h(x, y)$	aquifer thickness	$[L]$
$A(x, y)$	area upslope	$[L^2]$
$a(x, y)$	area upslope per unit contour width	$[L]$
$\theta(x, y)$	aquifer base slope angle	$[rad]$
h_g	characteristic geomorphic height scale	$[L]$
ℓ_g	characteristic geomorphic length scale	$[L]$
t_g	characteristic geomorphic time scale	$[T]$
h_c	characteristic hydrologic height scale	$[L]$
t_d	characteristic time to drain aquifer storage	$[T]$
E_f	fluvial incision rate	$[L/T]$
E_h	hillslope diffusion rate	$[L/T]$
U	uplift rate	$[L/T]$
K	streampower incision coefficient	$[1/T]$
m	streampower area exponent	$[-]$
n	streampower slope exponent	$[-]$
v_0	characteristic contour width	$[L]$
τ	bed shear stress	$[M/LT^2]$
τ_c	critical bed shear stress	$[M/LT^2]$
k_e	erosivity coefficient	$[M^{-\beta} L^{1+\beta} T^{2\beta-1}]$
β	shear stress exponent	$[-]$
ρ_w	density of water	$[M/L^3]$
g	acceleration due to gravity	$[L/T^2]$
d_f	channel flow depth	$[L]$
C	Chezy coefficient	$[L^{1/2}/T]$
w	channel width	$[L]$
k_w	width coefficient	$[-]$
b	permeable thickness	$[L]$
q_h	hillslope sediment transport rate	$[L^2/T]$
D	hillslope diffusivity	$[L^2/T]$
k_{sf}	timestep scaling factor	$[-]$
$q(x, y, t)$	groundwater specific discharge	$[L^2/T]$
$q_s(x, y, t)$	local surface runoff	$[L/T]$
$Q(x, y, t)$	discharge	$[L^3/T]$
$Q^*(x, y, t)$	dimensionless discharge	$[-]$
p	recharge rate	$[L/T]$
k_s	hydraulic conductivity	$[L/T]$
n	drainable porosity	$[-]$
\mathcal{G}	step function	
\mathcal{R}	ramp function	

954

Acknowledgments

955

956 This work was supported by NSF grants EAR-2012264, EAR-1654194, ACI-1450409, EAR-
 957 1725774, and EAR-1831623. No original data is presented in this paper. The code used
 958 here is archived at <https://doi.org/10.5281/zenodo.4727916>. Model output files will
 959 be archived and available prior to final publication.

References

960

961

962

963

964

965

966

967

968

969

970

971

972

973

974

975

976

977

978

979

980

981

982

983

984

985

986

987

988

989

990

991

992

993

994

995

996

997

998

999

1000

1001

1002

1003

1004

1005

1006

1007

1008

1009

1010

1011

1012

1013

1014

- Abrams, D. M., Lobkovsky, A. E., Petroff, A. P., Straub, K. M., McElroy, B., Mohrig, D. C., . . . Rothman, D. H. (2009, March). Growth laws for channel networks incised by groundwater flow. *Nature Geoscience*, *2*(3), 193–196. Retrieved 2019-11-11, from <http://www.nature.com/articles/ngeo432> doi: 10.1038/ngeo432
- Ahnert, F. (1976). Brief description of a comprehensive three-dimensional process-response model of landform development. *Zeitschrift für Geomorphologie, Supplement*, *25*, 29–49.
- Antonelli, M., Glaser, B., Teuling, A. J., Klaus, J., & Pfister, L. (2020, March). Saturated areas through the lens: 1. Spatio-temporal variability of surface saturation documented through thermal infrared imagery. *Hydrological Processes*, *34*(6), 1310–1332. Retrieved 2021-03-26, from <https://onlinelibrary.wiley.com/doi/abs/10.1002/hyp.13698> doi: 10.1002/hyp.13698
- Armstrong, A. (1976). A three-dimensional simulation of slope forms. *Zeitschrift für Geomorphologie, Supplement*, *25*, 20–28.
- Barenblatt, G. I. (1996). *Scaling, self-similarity, and intermediate asymptotics* (No. 14). Cambridge ; New York: Cambridge University Press.
- Barnhart, K. R., Hutton, E. W. H., Tucker, G. E., Gasparini, N. M., Istanbuloglu, E., Hobley, D. E. J., . . . Bandaragoda, C. (2020, May). Short communication: Landlab v2.0: a software package for Earth surface dynamics. *Earth Surface Dynamics*, *8*(2), 379–397. Retrieved 2020-11-27, from <https://esurf.copernicus.org/articles/8/379/2020/> (Publisher: Copernicus GmbH) doi: <https://doi.org/10.5194/esurf-8-379-2020>
- Barnhart, K. R., Tucker, G. E., Doty, S. G., Glade, R. C., Shobe, C. M., Rossi, M. W., & Hill, M. C. (2020). Projections of Landscape Evolution on a 10,000 Year Timescale With Assessment and Partitioning of Uncertainty Sources. *Journal of Geophysical Research: Earth Surface*, *125*(12), e2020JF005795. Retrieved 2021-01-05, from <http://agupubs.onlinelibrary.wiley.com/doi/abs/10.1029/2020JF005795> (eprint: <https://onlinelibrary.wiley.com/doi/pdf/10.1029/2020JF005795>) doi: <https://doi.org/10.1029/2020JF005795>
- Barnhart, K. R., Tucker, G. E., Doty, S. G., Shobe, C. M., Glade, R. C., Rossi, M. W., & Hill, M. C. (2020). Inverting Topography for Landscape Evolution Model Process Representation: 3. Determining Parameter Ranges for Select Mature Geomorphic Transport Laws and Connecting Changes in Fluvial Erodibility to Changes in Climate. *Journal of Geophysical Research: Earth Surface*, *125*(7), e2019JF005287. Retrieved 2020-07-08, from <http://agupubs.onlinelibrary.wiley.com/doi/abs/10.1029/2019JF005287> (eprint: <https://onlinelibrary.wiley.com/doi/pdf/10.1029/2019JF005287>) doi: 10.1029/2019JF005287
- Beven, K. J., & Kirkby, M. J. (1979). A physically based, variable contributing area model of basin hydrology. *Hydrological Sciences Bulletin*, *24*(1), 43–69. (ISBN: 0262666790) doi: 10.1080/02626667909491834
- Bishop, P. (2007). Long-term landscape evolution: linking tectonics and surface processes. *Earth Surface Processes and Landforms*, *32*(3), 329–365. Retrieved 2021-04-11, from <http://onlinelibrary.wiley.com/doi/abs/10.1002/esp.1493> (eprint: <https://onlinelibrary.wiley.com/doi/pdf/10.1002/esp.1493>) doi: <https://doi.org/10.1002/esp.1493>
- Bonetti, S., Bragg, A. D., & Porporato, A. (2018, March). On the theory of drainage area for regular and non-regular points. *Proceedings of the Royal Society A: Mathematical, Physical and Engineering Sciences*, *474*(2211), 20170693. Retrieved 2021-01-13, from <https://royalsocietypublishing.org/doi/full/10.1098/rspa.2017.0693> (Publisher: Royal Society) doi: 10.1098/rspa.2017.0693

- 1015 Bonetti, S., Hooshyar, M., Camporeale, C., & Porporato, A. (2020, January).
 1016 Channelization cascade in landscape evolution. *Proceedings of the Na-*
 1017 *tional Academy of Sciences*, 117(3), 1375–1382. Retrieved 2020-12-02, from
 1018 <https://www.pnas.org/content/117/3/1375> (Publisher: National Academy
 1019 of Sciences Section: Physical Sciences) doi: 10.1073/pnas.1911817117
- 1020 Brantley, S. L., Eissenstat, D. M., Marshall, J. A., Godsey, S. E., Balogh-Brunstad,
 1021 Z., Karwan, D. L., . . . Weathers, K. C. (2017). Reviews and syntheses: On
 1022 the roles trees play in building and plumbing the critical zone. *Biogeosciences*,
 1023 14(22), 5115–5142. doi: 10.5194/bg-14-5115-2017
- 1024 Brantley, S. L., Lebedeva, M. I., Balashov, V. N., Singha, K., Sullivan, P. L., &
 1025 Stinchcomb, G. (2017, January). Toward a conceptual model relating chemical
 1026 reaction fronts to water flow paths in hills. *Geomorphology*, 277, 100–117.
 1027 Retrieved 2019-11-13, from [https://linkinghub.elsevier.com/retrieve/
 1028 pii/S0169555X16308674](https://linkinghub.elsevier.com/retrieve/pii/S0169555X16308674) doi: 10.1016/j.geomorph.2016.09.027
- 1029 Braun, J., & Willett, S. D. (2013). A very efficient O(n), implicit and par-
 1030 allel method to solve the stream power equation governing fluvial inci-
 1031 sion and landscape evolution. *Geomorphology*, 180-181, 170–179. Re-
 1032 trieved from <http://dx.doi.org/10.1016/j.geomorph.2012.10.008> doi:
 1033 10.1016/j.geomorph.2012.10.008
- 1034 Brocca, L., Melone, F., Moramarco, T., & Singh, V. P. (2009, February). As-
 1035 similation of Observed Soil Moisture Data in Storm Rainfall-Runoff Mod-
 1036 eling. *Journal of Hydrologic Engineering*, 14(2), 153–165. doi: 10.1061/
 1037 (ASCE)1084-0699(2009)14:2(153)
- 1038 Brutsaert, W. (2005). *Hydrology: An Introduction*. Cambridge University Press. Re-
 1039 trieved from https://books.google.com/books?id=yX\ _xS55xyoC
- 1040 Carlston, C. W. (1963). *Drainage density and streamflow*. U.S. Govt. Print. Off.
 1041 (Google-Books-ID: FLsvAAAAYAAJ)
- 1042 Chen, A., Darbon, J., & Morel, J.-M. (2014, August). Landscape evolution models:
 1043 A review of their fundamental equations. *Geomorphology*, 219, 68–86. Re-
 1044 trieved 2020-12-03, from [http://www.sciencedirect.com/science/article/
 1045 pii/S0169555X14002402](http://www.sciencedirect.com/science/article/pii/S0169555X14002402) doi: 10.1016/j.geomorph.2014.04.037
- 1046 Childs, E. C. (1971). Drainage of Groundwater Resting on a Sloping Bed. *Water*
 1047 *Resources Research*, 7(5), 1256–1263. Retrieved 2019-11-11, from [https://
 1048 agupubs.onlinelibrary.wiley.com/doi/abs/10.1029/WR007i005p01256](https://agupubs.onlinelibrary.wiley.com/doi/abs/10.1029/WR007i005p01256)
 1049 doi: 10.1029/WR007i005p01256
- 1050 Deal, E., Braun, J., & Botter, G. (2018). Understanding the Role of Rainfall and
 1051 Hydrology in Determining Fluvial Erosion Efficiency. *Journal of Geophysical*
 1052 *Research: Earth Surface*, 123(4), 744–778. doi: 10.1002/2017JF004393
- 1053 Dietrich, W. E., Bellugi, D. G., Sklar, L. S., Stock, J. D., Heimsath, A. M., & Roer-
 1054 ing, J. J. (2003). Geomorphic Transport Laws for Predicting Landscape form
 1055 and Dynamics. In P. R. Wilcock & R. M. Iverson (Eds.), *Geophysical Mono-*
 1056 *graph Series* (pp. 103–132). Washington, D. C: American Geophysical Union.
 1057 Retrieved 2021-02-09, from <http://doi.wiley.com/10.1029/135GM09> doi:
 1058 10.1029/135GM09
- 1059 Dietrich, W. E., Wilson, C. J., Montgomery, D. R., & McKean, J. (1993, March).
 1060 Analysis of Erosion Thresholds, Channel Networks, and Landscape Morphol-
 1061 ogy Using a Digital Terrain Model. *The Journal of Geology*, 101(2), 259–278.
 1062 Retrieved 2021-04-09, from [https://www.journals.uchicago.edu/doi/
 1063 abs/10.1086/648220](https://www.journals.uchicago.edu/doi/abs/10.1086/648220) (Publisher: The University of Chicago Press) doi:
 1064 10.1086/648220
- 1065 Dunne, T. (1978). Field studies of hillslope flow processes. In *Hillslope Hydrology*.
 1066 Dunne, T., & Black, R. D. (1970). Partial Area Contributions to Storm Runoff in
 1067 a Small New England Watershed. *Water Resources Research*, 6(5), 1296–1311.
 1068 (ISBN: 0043-1397) doi: 10.1029/WR006i005p01296
- 1069 Forte, A. M., Yanites, B. J., & Whipple, K. X. (2016). Complexities of landscape

- 1070 evolution during incision through layered stratigraphy with contrasts in rock
 1071 strength. *Earth Surface Processes and Landforms*, 41(12), 1736–1757. Re-
 1072 trieved 2020-01-20, from [https://onlinelibrary.wiley.com/doi/abs/](https://onlinelibrary.wiley.com/doi/abs/10.1002/esp.3947)
 1073 [10.1002/esp.3947](https://onlinelibrary.wiley.com/doi/abs/10.1002/esp.3947) doi: 10.1002/esp.3947
- 1074 Gabet, E. J., & Mudd, S. M. (2009). A theoretical model coupling chemical weath-
 1075 ering rates with denudation rates. *Geology*, 37(2), 151–154. doi: 10.1130/
 1076 G25270A.1
- 1077 Gabet, E. J., & Mudd, S. M. (2010). Bedrock erosion by root fracture and tree
 1078 throw: A coupled biogeomorphic model to explore the humped soil produc-
 1079 tion function and the persistence of hillslope soils. *Journal of Geophysical*
 1080 *Research: Earth Surface*, 115(F4). Retrieved 2020-01-10, from [https://](https://agupubs.onlinelibrary.wiley.com/doi/abs/10.1029/2009JF001526)
 1081 agupubs.onlinelibrary.wiley.com/doi/abs/10.1029/2009JF001526 doi:
 1082 [10.1029/2009JF001526](https://agupubs.onlinelibrary.wiley.com/doi/abs/10.1029/2009JF001526)
- 1083 Harman, C., & Sivapalan, M. (2009). A similarity framework to assess controls
 1084 on shallow subsurface flow dynamics in hillslopes. *Water Resources Research*,
 1085 45(1), 1–12. doi: 10.1029/2008WR007067
- 1086 Harman, C., & Troch, P. A. (2014, February). What makes Darwinian hydrolog-
 1087 ogy "Darwinian"? Asking a different kind of question about landscapes.
 1088 *Hydrology and Earth System Sciences*, 18(2), 417–433. Retrieved 2020-01-
 1089 22, from <https://www.hydrol-earth-syst-sci.net/18/417/2014/> doi:
 1090 [10.5194/hess-18-417-2014](https://www.hydrol-earth-syst-sci.net/18/417/2014/)
- 1091 Harman, C. J., & Cosans, C. L. (2019). A low-dimensional model of bedrock weath-
 1092 ering and lateral flow coevolution in hillslopes: 2. Controls on weathering and
 1093 permeability profiles, drainage hydraulics, and solute export pathways. *Hydro-*
 1094 *logical Processes*(December 2018), 1168–1190. doi: 10.1002/hyp.13385
- 1095 Harman, C. J., & Kim, M. (2019). A low-dimensional model of bedrock weath-
 1096 ering and lateral flow coevolution in hillslopes: 1. Hydraulic theory of re-
 1097 active transport. *Hydrological Processes*, 33(4), 466–475. Retrieved from
 1098 <https://onlinelibrary.wiley.com/doi/pdf/10.1002/hyp.13360> doi:
 1099 [10.1002/hyp.13360](https://onlinelibrary.wiley.com/doi/pdf/10.1002/hyp.13360)
- 1100 Hewlett, J. D., & Hibbert, A. R. (1967). Factors affecting the response of small wa-
 1101 tersheds to precipitation in humid areas. In *Int. Symp. Forest Hydrology*. doi:
 1102 [10.1177/0309133309338118](https://doi.org/10.1177/0309133309338118)
- 1103 Hobley, D. E. J., Adams, J. M., Nudurupati, S. S., Hutton, E. W. H., Gasparini,
 1104 N. M., Istanbuluoglu, E., & Tucker, G. E. (2017). Creative computing
 1105 with Landlab: an open-source toolkit for building, coupling, and exploring
 1106 two-dimensional numerical models of Earth-surface dynamics. , 21–46. doi:
 1107 [10.5194/esurf-5-21-2017](https://doi.org/10.5194/esurf-5-21-2017)
- 1108 Horton, R. E. (1945, March). Erosional development of streams and their drainage
 1109 basins; hydrophysical approach to quantitative morphology. *GSA Bul-*
 1110 *letin*, 56(3), 275–370. Retrieved from [https://doi.org/10.1130/0016-](https://doi.org/10.1130/0016-7606(1945)56[275:EDOSAT]2.0.CO)
 1111 [7606\(1945\)56\[275:EDOSAT\]2.0.CO](https://doi.org/10.1130/0016-7606(1945)56[275:EDOSAT]2.0.CO) doi: 10.1130/0016-7606(1945)56[275:
 1112 [EDOSAT\]2.0.CO;2](https://doi.org/10.1130/0016-7606(1945)56[275:EDOSAT]2.0.CO)
- 1113 Howard, A. D. (1994). A detachment-limited model of drainage basin evolution.
 1114 *Water Resources Research*, 30(7), 2261–2285. Retrieved 2020-01-16, from
 1115 <https://agupubs.onlinelibrary.wiley.com/doi/abs/10.1029/94WR00757>
 1116 doi: 10.1029/94WR00757
- 1117 Howard, A. D., & Kerby, G. (1983, June). Channel changes in badlands.
 1118 *GSA Bulletin*, 94(6), 739–752. Retrieved 2020-01-20, from [https://](https://pubs.geoscienceworld.org/gsabulletin/article/94/6/739/202874/Channel-changes-in-badlands)
 1119 [pubs.geoscienceworld.org/gsabulletin/article/94/6/739/202874/](https://pubs.geoscienceworld.org/gsabulletin/article/94/6/739/202874/Channel-changes-in-badlands)
 1120 [Channel-changes-in-badlands](https://pubs.geoscienceworld.org/gsabulletin/article/94/6/739/202874/Channel-changes-in-badlands) doi: 10.1130/0016-7606(1983)94(739:
 1121 [CCIB\)2.0.CO;2](https://pubs.geoscienceworld.org/gsabulletin/article/94/6/739/202874/Channel-changes-in-badlands)
- 1122 Huang, X., & Niemann, J. D. (2006). Modelling the potential impacts of groundwa-
 1123 ter hydrology on long-term drainage basin evolution. *Earth Surface Processes*
 1124 *and Landforms*. doi: 10.1002/esp.1369

- 1125 Huang, X., & Niemann, J. D. (2008). How do streamflow generation mechanisms af-
 1126 fect watershed hypsometry? *Earth Surface Processes and Landforms*. doi: 10
 1127 .1002/esp.1573
- 1128 Ijjász-Vásquez, E. J., Bras, R. L., & Moglen, G. E. (1992). Sensitivity of a basin
 1129 evolution model to the nature of runoff production and to initial conditions.
 1130 doi: 10.1029/92WR01561
- 1131 Jefferson, A., Grant, G. E., Lewis, S. L., & Lancaster, S. T. (2010). Coevolution
 1132 of hydrology and topography on a basalt landscape in the Oregon Cascade
 1133 Range, USA. *Earth Surface Processes and Landforms*, 35(7), 803–816. doi:
 1134 10.1002/esp.1976
- 1135 Lague, D., Hovius, N., & Davy, P. (2005, December). Discharge, discharge
 1136 variability, and the bedrock channel profile. *Journal of Geophysical Re-*
 1137 *search: Earth Surface*, 110(F4). Retrieved 2021-03-18, from [http://](http://agupubs.onlinelibrary.wiley.com/doi/full/10.1029/2004JF000259)
 1138 agupubs.onlinelibrary.wiley.com/doi/full/10.1029/2004JF000259
 1139 (Publisher: John Wiley & Sons, Ltd) doi: 10.1029/2004JF000259
- 1140 Laity, J. E., & Malin, M. C. (1985). Sapping processes and the development of
 1141 theater-headed valley networks on the Colorado Plateau. *Geological Society of*
 1142 *America Bulletin*, 96, 203–217.
- 1143 Lapides, D. A., David, C., Sytsma, A., Dralle, D., & Thompson, S. (2020, August).
 1144 Analytical Solutions To Runoff On Hillslopes With Curvature: Numerical And
 1145 Laboratory Verification. *Hydrological Processes*, hyp.13879. Retrieved 2020-08-
 1146 15, from <https://onlinelibrary.wiley.com/doi/abs/10.1002/hyp.13879>
 1147 doi: 10.1002/hyp.13879
- 1148 Leopold, L. B., & Maddock, T. (1953). *The Hydraulic Geometry of Stream Chan-*
 1149 *nels and Some Physiographic Implications*. U.S. Government Printing Office.
 1150 (Google-Books-ID: 4UGH22BKfdsC)
- 1151 Litwin, D., Tucker, G., Barnhart, K., & Harman, C. (2020, February). Groundwa-
 1152 terDupuitPercolator: A Landlab component for groundwater flow. *Journal of*
 1153 *Open Source Software*, 5(46), 1935. Retrieved 2020-02-11, from [https://joss](https://joss.theoj.org/papers/10.21105/joss.01935)
 1154 [.theoj.org/papers/10.21105/joss.01935](https://joss.theoj.org/papers/10.21105/joss.01935) doi: 10.21105/joss.01935
- 1155 Lohse, K. A., & Dietrich, W. E. (2005). Contrasting effects of soil development on
 1156 hydrological properties and flow paths. *Water Resources Research*, 41(12), 1–
 1157 17. doi: 10.1029/2004WR003403
- 1158 Longobardi, A., Villani, P., Grayson, R. B., & Western, A. W. (2003). On the
 1159 relationship between runoff coefficient and catchment initial conditions. *Mod-*
 1160 *elling and Simulation Society of Australia and New Zealand*, 2(1), 1–6. (ISBN:
 1161 1-74052-098-X)
- 1162 Luo, W., & Pederson, D. T. (2012). Hydraulic conductivity of the High
 1163 Plains Aquifer re-evaluated using surface drainage patterns. *Geophys-*
 1164 *ical Research Letters*, 39(2). Retrieved 2021-04-11, from [http://agupubs](http://agupubs.onlinelibrary.wiley.com/doi/abs/10.1029/2011GL050200)
 1165 [.onlinelibrary.wiley.com/doi/abs/10.1029/2011GL050200](http://agupubs.onlinelibrary.wiley.com/doi/abs/10.1029/2011GL050200) (eprint:
 1166 <https://onlinelibrary.wiley.com/doi/pdf/10.1029/2011GL050200>) doi:
 1167 <https://doi.org/10.1029/2011GL050200>
- 1168 Martin, Y., & Church, M. (2004, September). Numerical modelling of landscape evo-
 1169 lution: geomorphological perspectives. *Progress in Physical Geography: Earth*
 1170 *and Environment*, 28(3), 317–339. Retrieved 2021-04-11, from [https://doi](https://doi.org/10.1191/0309133304pp412ra)
 1171 [.org/10.1191/0309133304pp412ra](https://doi.org/10.1191/0309133304pp412ra) (Publisher: SAGE Publications Ltd) doi:
 1172 10.1191/0309133304pp412ra
- 1173 Marçais, J., de Dreuzy, J. R., & Erhel, J. (2017). Dynamic coupling of subsurface
 1174 and seepage flows solved within a regularized partition formulation. *Advances*
 1175 *in Water Resources*, 109, 94–105. doi: 10.1016/j.advwatres.2017.09.008
- 1176 Montgomery, D. R., & Dietrich, W. E. (1994, April). A physically based
 1177 model for the topographic control on shallow landsliding. *Water Re-*
 1178 *sources Research*, 30(4), 1153–1171. Retrieved 2021-02-02, from [http://](http://agupubs.onlinelibrary.wiley.com/doi/abs/10.1029/93WR02979)
 1179 agupubs.onlinelibrary.wiley.com/doi/abs/10.1029/93WR02979 (Pub-

- lisher: John Wiley & Sons, Ltd) doi: 10.1029/93WR02979
- 1180
1181 Nippgen, F., McGlynn, B. L., & Emanuel, R. E. (2015). The spatial and tempo-
1182 ral evolution of contributing areas. *Water Resources Research*. doi: 10.1002/
1183 2014WR016719
- 1184 O'Loughlin, E. M. (1981). Saturation regions in catchments and their relations
1185 to soil and topographic properties. *Journal of Hydrology*, 53(3-4), 229–246.
1186 (ISBN: 0022-1694) doi: 10.1016/0022-1694(81)90003-2
- 1187 Pazzaglia, F. J. (2003, January). Landscape evolution models. In *Develop-*
1188 *ments in Quaternary Sciences* (Vol. 1, pp. 247–274). Elsevier. Retrieved
1189 2021-04-11, from [https://www.sciencedirect.com/science/article/pii/](https://www.sciencedirect.com/science/article/pii/S1571086603010121)
1190 [S1571086603010121](https://www.sciencedirect.com/science/article/pii/S1571086603010121) doi: 10.1016/S1571-0866(03)01012-1
- 1191 Pelletier, J. D. (2013, January). 2.3 Fundamental Principles and Techniques of
1192 Landscape Evolution Modeling. In J. F. Shroder (Ed.), *Treatise on Ge-*
1193 *omorphology* (pp. 29–43). San Diego: Academic Press. Retrieved 2021-
1194 04-11, from [https://www.sciencedirect.com/science/article/pii/](https://www.sciencedirect.com/science/article/pii/B9780123747396000257)
1195 [B9780123747396000257](https://www.sciencedirect.com/science/article/pii/B9780123747396000257) doi: 10.1016/B978-0-12-374739-6.00025-7
- 1196 Perron, J. T., Dietrich, W. E., & Kirchner, J. W. (2008). Controls on the spacing of
1197 first-order valleys. *Journal of Geophysical Research: Earth Surface*, 113(4), 1–
1198 21. doi: 10.1029/2007JF000977
- 1199 Prancevic, J. P., & Kirchner, J. W. (2019). Topographic controls on the exten-
1200 sion and retraction of flowing streams. *Geophysical Research Letters*, 0(0).
1201 Retrieved from [https://agupubs.onlinelibrary.wiley.com/doi/abs/](https://agupubs.onlinelibrary.wiley.com/doi/abs/10.1029/2018GL081799)
1202 [10.1029/2018GL081799](https://agupubs.onlinelibrary.wiley.com/doi/abs/10.1029/2018GL081799) doi: 10.1029/2018GL081799
- 1203 Rempe, D. M., & Dietrich, W. E. (2014, May). A bottom-up control on
1204 fresh-bedrock topography under landscapes. *Proceedings of the Na-*
1205 *tional Academy of Sciences*, 111(18), 6576–6581. Retrieved 2019-11-03,
1206 from <http://www.pnas.org/cgi/doi/10.1073/pnas.1404763111> doi:
1207 [10.1073/pnas.1404763111](http://www.pnas.org/cgi/doi/10.1073/pnas.1404763111)
- 1208 Roering, J. J. (2008, September). How well can hillslope evolution models "explain"
1209 topography? Simulating soil transport and production with high-resolution
1210 topographic data. *Geological Society of America Bulletin*, 120(9-10), 1248–
1211 1262. Retrieved 2019-09-19, from [https://pubs.geoscienceworld.org/](https://pubs.geoscienceworld.org/gsabulletin/article/120/9-10/1248-1262/2317)
1212 [gsabulletin/article/120/9-10/1248-1262/2317](https://pubs.geoscienceworld.org/gsabulletin/article/120/9-10/1248-1262/2317) doi: 10.1130/B26283.1
- 1213 Roering, J. J., Kirchner, J. W., & Dietrich, W. E. (1999). Evidence for nonlin-
1214 ear, diffusive sediment transport on hillslopes and implications for land-
1215 scape morphology. *Water Resources Research*, 35(3), 853–870. doi:
1216 [10.1029/1998WR900090](https://doi.org/10.1029/1998WR900090)
- 1217 Roering, J. J., Kirchner, J. W., & Dietrich, W. E. (2001, August). Hillslope evo-
1218 lution by nonlinear, slope-dependent transport: Steady state morphology
1219 and equilibrium adjustment timescales. *Journal of Geophysical Research:*
1220 *Solid Earth*, 106(B8), 16499–16513. Retrieved 2021-04-20, from [http://](http://agupubs.onlinelibrary.wiley.com/doi/abs/10.1029/2001jb000323)
1221 agupubs.onlinelibrary.wiley.com/doi/abs/10.1029/2001jb000323 (Pub-
1222 lisher: John Wiley & Sons, Ltd) doi: 10.1029/2001JB000323
- 1223 Rosenbloom, N. A., & Anderson, R. S. (1994, July). Hillslope and channel
1224 evolution in a marine terraced landscape, Santa Cruz, California. *Jour-*
1225 *nal of Geophysical Research: Solid Earth*, 99(B7), 14013–14029. Re-
1226 trieved 2019-09-26, from [https://agupubs.onlinelibrary.wiley.com/](https://agupubs.onlinelibrary.wiley.com/doi/10.1029/94JB00048@10.1002/(ISSN)2169-9356.TECTOP1)
1227 [doi/10.1029/94JB00048@10.1002/\(ISSN\)2169-9356.TECTOP1](https://agupubs.onlinelibrary.wiley.com/doi/10.1029/94JB00048@10.1002/(ISSN)2169-9356.TECTOP1) doi:
1228 [10.1029/94JB00048@10.1002/\(ISSN\)2169-9356.TECTOP1](https://doi.org/10.1029/94JB00048@10.1002/(ISSN)2169-9356.TECTOP1)
- 1229 Snyder, N. P., Whipple, K. X., Tucker, G. E., & Merritts, D. J. (2003, July).
1230 Channel response to tectonic forcing: field analysis of stream morphology
1231 and hydrology in the Mendocino triple junction region, northern Califor-
1232 nia. *Geomorphology*, 53(1), 97–127. Retrieved 2021-04-21, from [https://](https://www.sciencedirect.com/science/article/pii/S0169555X02003495)
1233 www.sciencedirect.com/science/article/pii/S0169555X02003495 doi:
1234 [10.1016/S0169-555X\(02\)00349-5](https://doi.org/10.1016/S0169-555X(02)00349-5)

- 1235 Tarboton, D. G., Bras, R. L., & Rodriguez-Iturbe, I. (1989, September). Scaling
1236 and elevation in river networks. *Water Resources Research*, *25*(9), 2037–2051.
1237 Retrieved 2021-04-09, from [http://agupubs.onlinelibrary.wiley.com/doi/](http://agupubs.onlinelibrary.wiley.com/doi/abs/10.1029/WR025i009p02037)
1238 [abs/10.1029/WR025i009p02037](http://agupubs.onlinelibrary.wiley.com/doi/abs/10.1029/WR025i009p02037) (Publisher: John Wiley & Sons, Ltd) doi:
1239 10.1029/WR025i009p02037
- 1240 Temme, A. J. A. M., Schoorl, J. M., Claessens, L., & Veldkamp, A. (2013, January).
1241 2.13 Quantitative Modeling of Landscape Evolution. In J. F. Shroder (Ed.),
1242 *Treatise on Geomorphology* (pp. 180–200). San Diego: Academic Press. doi:
1243 10.1016/B978-0-12-374739-6.00039-7
- 1244 Theodoratos, N., & Kirchner, J. W. (2020a, June). Dimensional analysis of a land-
1245 scape evolution model with incision threshold. *Earth Surface Dynamics*, *8*(2),
1246 505–526. Retrieved 2020-06-04, from [https://www.earth-surf-dynam.net/8/](https://www.earth-surf-dynam.net/8/505/2020/)
1247 [505/2020/](https://www.earth-surf-dynam.net/8/505/2020/) (Publisher: Copernicus GmbH) doi: [https://doi.org/10.5194/esurf](https://doi.org/10.5194/esurf-8-505-2020)
1248 [-8-505-2020](https://doi.org/10.5194/esurf-8-505-2020)
- 1249 Theodoratos, N., & Kirchner, J. W. (2020b, June). Graphically interpreting how
1250 incision thresholds influence topographic and scaling properties of modeled
1251 landscapes. *Earth Surface Dynamics Discussions*, 1–25. Retrieved 2021-04-15,
1252 from <https://esurf.copernicus.org/preprints/esurf-2020-45/> (Pub-
1253 lisher: Copernicus GmbH) doi: 10.5194/esurf-2020-45
- 1254 Theodoratos, N., Seybold, H., & Kirchner, J. W. (2018, September). Scaling and
1255 similarity of a stream-power incision and linear diffusion landscape evolution
1256 model. *Earth Surface Dynamics*, *6*(3), 779–808. Retrieved 2020-08-03, from
1257 <https://esurf.copernicus.org/articles/6/779/2018/> (Publisher: Copernicus
1258 GmbH) doi: <https://doi.org/10.5194/esurf-6-779-2018>
- 1259 Trambly, Y., Bouvier, C., Martin, C., Didon-Lescot, J.-F., Todorovik, D., & Domer-
1260 gue, J.-M. (2010, June). Assessment of initial soil moisture conditions for
1261 event-based rainfall–runoff modelling. *Journal of Hydrology*, *387*(3), 176–
1262 187. Retrieved 2020-01-08, from [http://www.sciencedirect.com/science/](http://www.sciencedirect.com/science/article/pii/S0022169410001873)
1263 [article/pii/S0022169410001873](http://www.sciencedirect.com/science/article/pii/S0022169410001873) doi: 10.1016/j.jhydrol.2010.04.006
- 1264 Troch, P. A., Lahmers, T., Meira, A., Mukherjee, R., Pedersen, J. W., Roy, T., &
1265 Valdes-Pineda, R. (2015). Catchment coevolution: A useful framework for
1266 improving predictions of hydrological change? *Water Resources Research*,
1267 *51*(7), 4903–4922. (arXiv: 10.1002/2014WR016527 ISBN: 6176273099) doi:
1268 10.1002/2015WR017032
- 1269 Troch, P. A., Paniconi, C., & Van Loon, E. E. (2003). Hillslope-storage Boussinesq
1270 model for subsurface flow and variable source areas along complex hillslopes:
1271 1. Formulation and characteristic response. *Water Resources Research*, *39*(11).
1272 doi: 10.1029/2002WR001728
- 1273 Tsujimoto, T. (1999). Sediment transport processes and channel incision: mixed size
1274 sediment transport, degradation and armoring. *Incised river channels*, 37–66.
1275 (Publisher: John Wiley Hoboken, NJ)
- 1276 Tucker, G. E. (2004). Drainage basin sensitivity to tectonic and climatic forcing: im-
1277 plications of a stochastic model for the role of entrainment and erosion thresh-
1278 olds. *Earth Surface Processes and Landforms*, *29*(2), 185–205. Retrieved 2020-
1279 01-20, from <https://onlinelibrary.wiley.com/doi/abs/10.1002/esp.1020>
1280 doi: 10.1002/esp.1020
- 1281 Tucker, G. E., & Bras, R. L. (1998). Hillslope processes, drainage density, and land-
1282 scape morphology. *Water Resources Research*, *34*(10), 2751–2764. Retrieved
1283 from <http://doi.wiley.com/10.1029/98WR01474> doi: 10.1029/98WR01474
- 1284 Tucker, G. E., Catani, F., Rinaldo, A., & Bras, R. L. (2001, February). Statisti-
1285 cal analysis of drainage density from digital terrain data. *Geomorphology*,
1286 *36*(3), 187–202. Retrieved 2019-09-25, from [http://www.sciencedirect.com/](http://www.sciencedirect.com/science/article/pii/S0169555X00000568)
1287 [science/article/pii/S0169555X00000568](http://www.sciencedirect.com/science/article/pii/S0169555X00000568) doi: 10.1016/S0169-555X(00)
1288 00056-8

- 1289 Tucker, G. E., & Slingerland, R. (1997). Drainage basin responses to climate change.
 1290 *Water Resources Research*, *33*(8), 2031–2047. Retrieved 2020-01-09, from
 1291 <https://agupubs.onlinelibrary.wiley.com/doi/abs/10.1029/97WR00409>
 1292 doi: 10.1029/97WR00409
- 1293 Valters, D. (2016, May). Modelling Geomorphic Systems: Landscape Evolution. In
 1294 (p. 6.5.12). doi: 10.13140/RG.2.1.1970.9047
- 1295 West, A. J., Galy, A., & Bickle, M. (2005, June). Tectonic and climatic controls
 1296 on silicate weathering. *Earth and Planetary Science Letters*, *235*(1), 211–
 1297 228. Retrieved 2021-02-10, from [https://www.sciencedirect.com/science/](https://www.sciencedirect.com/science/article/pii/S0012821X05002116)
 1298 [article/pii/S0012821X05002116](https://www.sciencedirect.com/science/article/pii/S0012821X05002116) doi: 10.1016/j.epsl.2005.03.020
- 1299 Whipple, K. X. (2001, April). Fluvial Landscape Response Time: How Plausi-
 1300 ble Is Steady-State Denudation? *American Journal of Science*, *301*(4-5), 313–
 1301 325. Retrieved 2021-01-11, from [https://www.ajsonline.org/content/301/](https://www.ajsonline.org/content/301/4-5/313)
 1302 [4-5/313](https://www.ajsonline.org/content/301/4-5/313) (Publisher: American Journal of Science Section: ARTICLES) doi:
 1303 10.2475/ajs.301.4-5.313
- 1304 Whipple, K. X., Hancock, G. S., & Anderson, R. S. (2000). River incision into
 1305 bedrock: Mechanics and relative efficacy of plucking, abrasion and cavitation.
 1306 *Geological Society of America Bulletin*, *18*.
- 1307 Whipple, K. X., & Tucker, G. E. (1999). Dynamics of the stream-power river in-
 1308 cision model: Implications for height limits of mountain ranges, landscape
 1309 response timescales, and research needs. *Journal of Geophysical Research:*
 1310 *Solid Earth*, *104*(B8), 17661–17674. Retrieved 2019-11-03, from [https://](https://agupubs.onlinelibrary.wiley.com/doi/abs/10.1029/1999JB900120)
 1311 agupubs.onlinelibrary.wiley.com/doi/abs/10.1029/1999JB900120 doi:
 1312 10.1029/1999JB900120
- 1313 Willgoose, G., Bras, R. L., & Rodriguez-Iturbe, I. (1991, July). A physi-
 1314 cal explanation of an observed link area-slope relationship. *Water Re-*
 1315 *sources Research*, *27*(7), 1697–1702. Retrieved 2021-04-09, from [http://](http://agupubs.onlinelibrary.wiley.com/doi/abs/10.1029/91WR00937)
 1316 agupubs.onlinelibrary.wiley.com/doi/abs/10.1029/91WR00937 (Pub-
 1317 lisher: John Wiley & Sons, Ltd) doi: 10.1029/91WR00937
- 1318 Willgoose, G., Bras, R. L., & Rodriguez-Iturbe, I. (1991). A coupled channel
 1319 network growth and hillslope evolution model: 1. Theory. *Water Resources*
 1320 *Research*, *1671*–1684. doi: 10.1029/91WR00935@10.1002/(ISSN)1944-7973
 1321 .USALPINE1
- 1322 Wohl, E., & David, G. C. L. (2008). Consistency of scaling relations among
 1323 bedrock and alluvial channels. *Journal of Geophysical Research: Earth Sur-*
 1324 *face*, *113*(F4). Retrieved 2021-04-09, from [http://agupubs.onlinelibrary](http://agupubs.onlinelibrary.wiley.com/doi/abs/10.1029/2008JF000989)
 1325 [.wiley.com/doi/abs/10.1029/2008JF000989](http://agupubs.onlinelibrary.wiley.com/doi/abs/10.1029/2008JF000989) doi: [https://doi.org/10.1029/](https://doi.org/10.1029/2008JF000989)
 1326 [2008JF000989](https://doi.org/10.1029/2008JF000989)
- 1327 Yoshida, T., & Troch, P. A. (2016). Coevolution of volcanic catchments in Japan.
 1328 *Hydrology and Earth System Sciences*, *20*(3), 1133–1150. (ISBN: 1607-7938)
 1329 doi: 10.5194/hess-20-1133-2016
- 1330 Zhang, Y., Slingerland, R., & Duffy, C. (2016). Fully-coupled hydrologic pro-
 1331 cesses for modeling landscape evolution. *Environmental Modelling and*
 1332 *Software*, *82*, 89–107. Retrieved from [http://dx.doi.org/10.1016/](http://dx.doi.org/10.1016/j.envsoft.2016.04.014)
 1333 [j.envsoft.2016.04.014](http://dx.doi.org/10.1016/j.envsoft.2016.04.014) doi: 10.1016/j.envsoft.2016.04.014

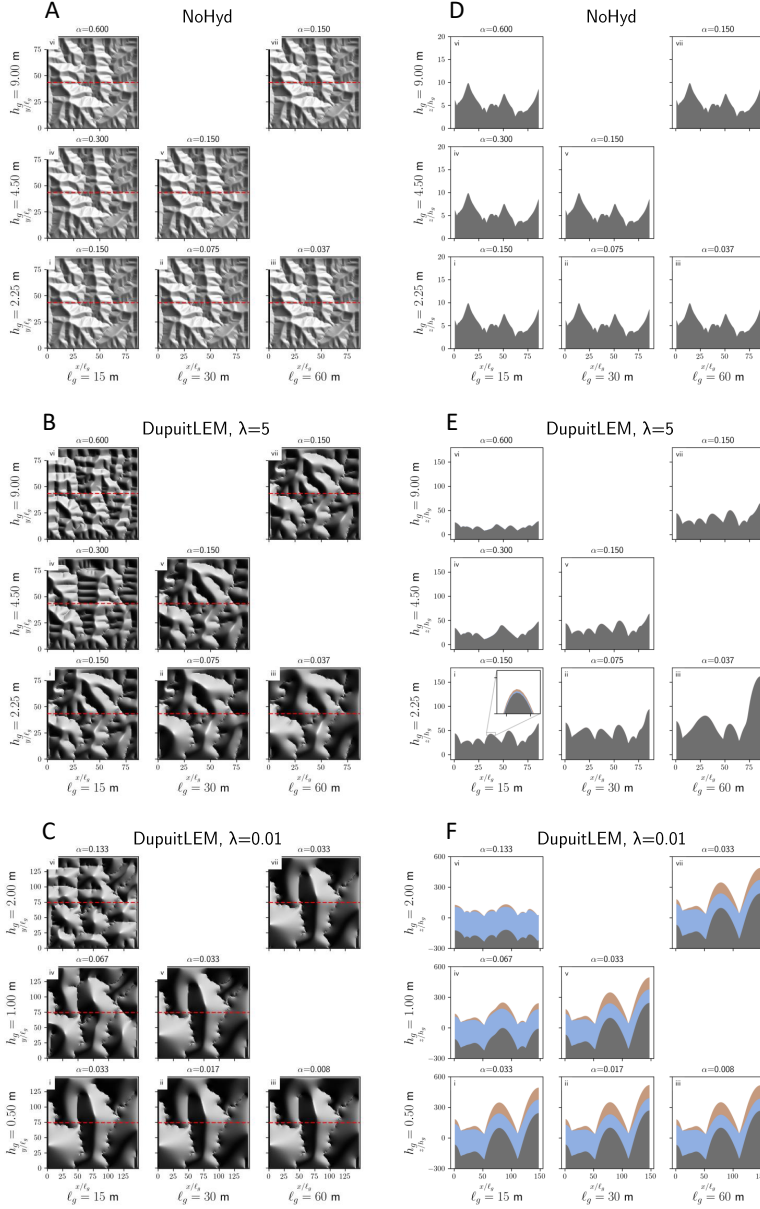


Figure 1. Hillshade plots (A, B, C) and cross sections (D, E, F) of steady state elevation for model runs with varying h_g and l_g . Cross sections are taken along the dashed red lines. Data plotted are in the re-scaled coordinate system (x', y', z') . (A, D) Model runs with the *NoHyd* model, showing topography is nearly identical between the runs in the dimensionless coordinate system regardless of the chosen values of h_g and l_g . (B, E) *DupuitLEM* model results are sensitive to independent scaling of l_g ($i \rightarrow ii \rightarrow iii$) and h_g ($i \rightarrow iv \rightarrow vi$) when Hi is large. Scaling such that $\alpha = h_g/l_g$ remains constant produces topography that is similar in the re-scaled coordinates. (C, F) *DupuitLEM* results with small Hi , showing reduced sensitivity of modeled topography to chosen length scales for small values of α . Note that the dimensionless size of the domain in the $Hi = 0.01$ cases is larger than the other cases in order to resolve a sufficient number of ridge-valley features. This was accomplished by maintaining the number of grid cells and increasing the contour width v_0 . The values of h_g in the $Hi = 0.01$ cases (C, F) are also smaller to allow for achievement of a tractable solution with very small Hi . Cross sections show the impermeable base elevation, water table elevation, and topographic elevation. Here zero elevation is the fixed topographic elevation boundary condition along the lower edge of the domain.

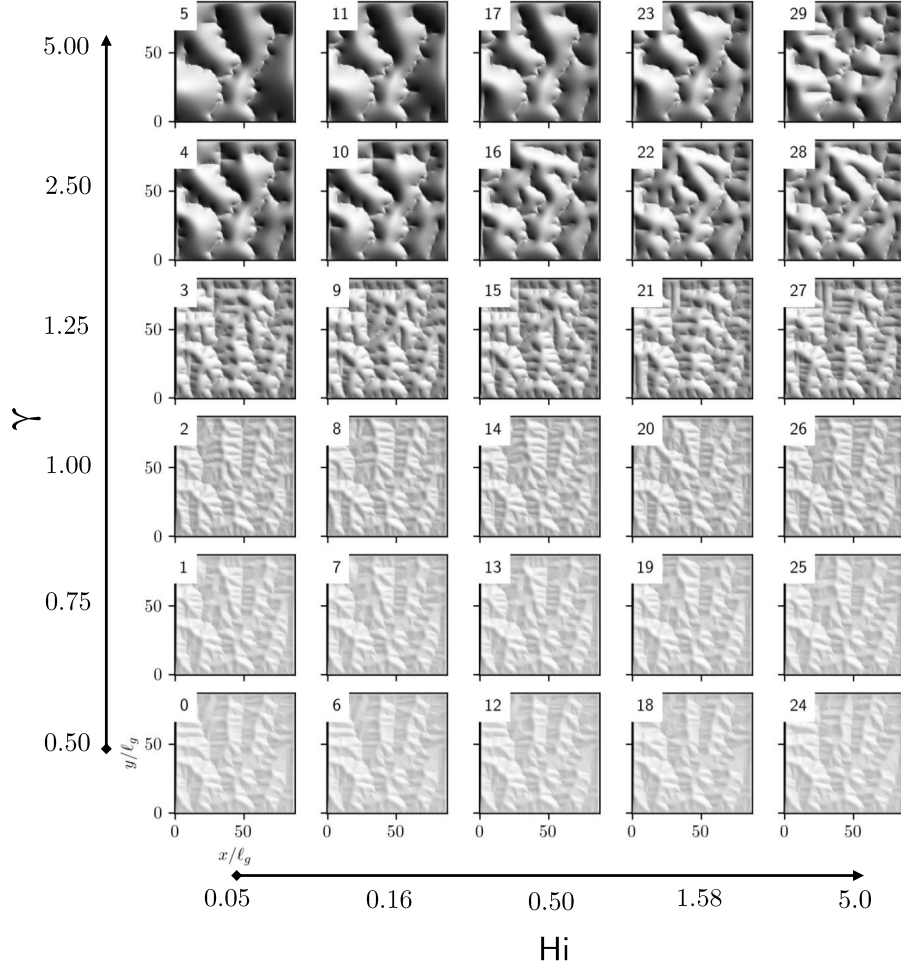


Figure 2. Hillshade plots of steady state elevation using the *DupuitLEM* model varying γ and Hi while α is held constant. Hi varies over two orders of magnitude on a geometric scale, while γ varies over one order of magnitude, further subdivided to show the transition that occurs at $\gamma = 1$. Low γ topography appears similar to *NoHyd* model results, and is less sensitive to varying Hi . Large γ results show broad hillslopes and slightly greater sensitivity to Hi .

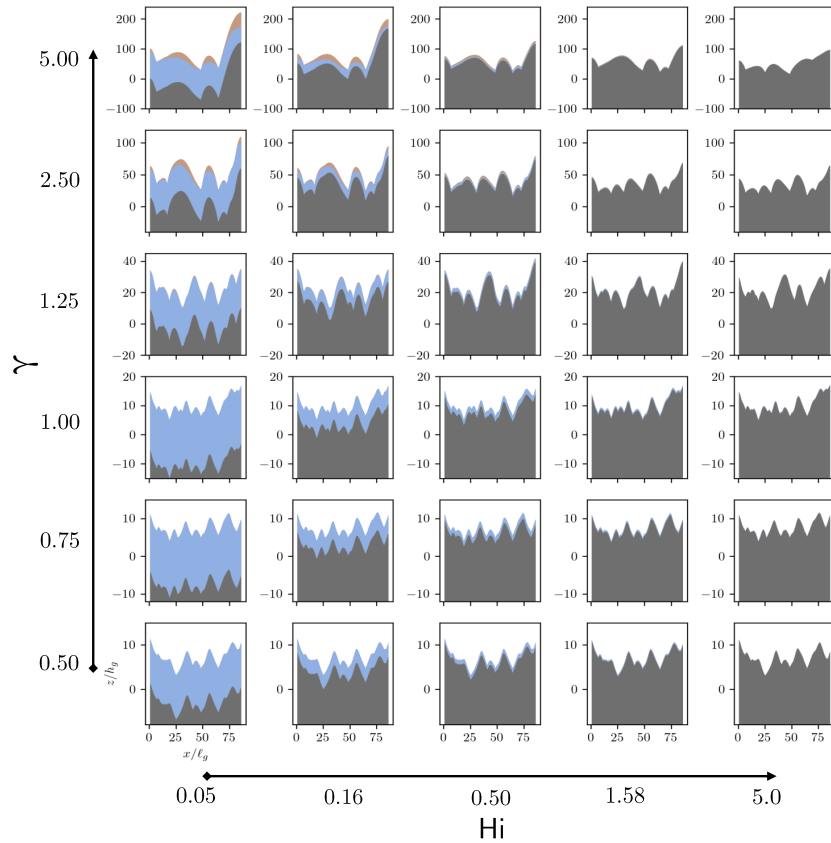


Figure 3. Cross section plots of *DupuitLEM* model results with varying γ and H_i corresponding to hillshades in 2. Cross sections are taken in the same fashion to 1, horizontally along the midpoint of the domain. Despite apparent similarities of the hillshades, there are prominent differences in the subsurface with varying H_i . Lower H_i cases will have deeper regolith, as this is dependent on the value of H_i . Noticeable depth to water table only becomes apparent at large values of γ .

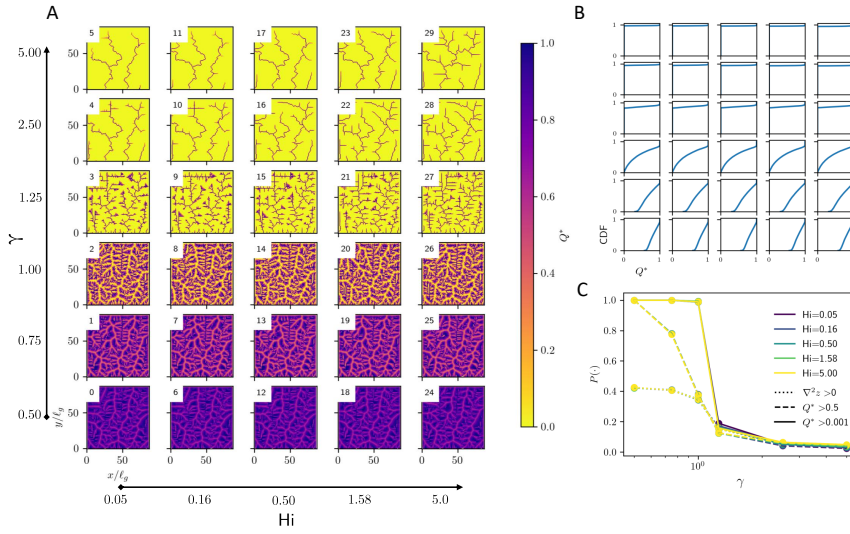


Figure 4. (A) Spatial patterns of Q^* from the *DupuitLEM* model varying γ and H_i while all other parameters are held constant. Results are similar across differences in H_i , but show significant differences with γ . All points in the landscape generate some runoff in the lowest *gamma* trials. (B) Cumulative distribution functions of Q^* with varying γ and H_i . Low γ trials show a range of Q^* values, with all areas contributing to some degree. High γ cases show most areas do not contribute runoff, with a small number where $Q^* \approx 1$. (C) Proportion of nodes contributing runoff at $Q^* > 0.5$, with varying γ (x-axis) and H_i (colors). Extent of areas contributing runoff is small for large H_i , and generally decreases with decreasing H_i .

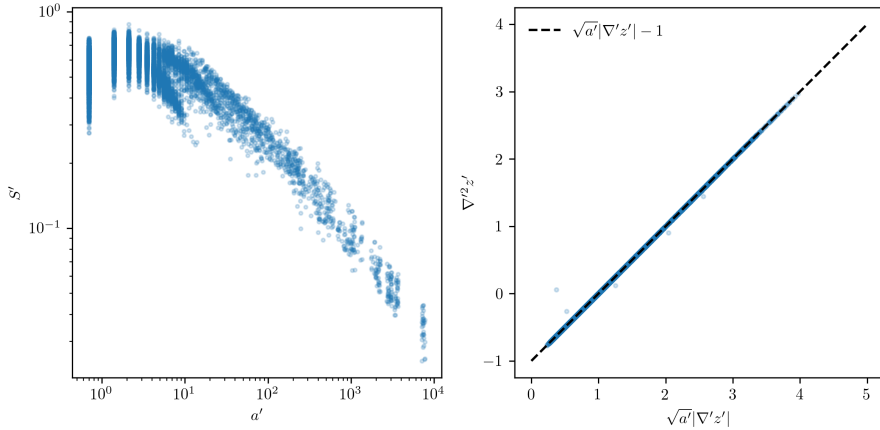


Figure 5. Dimensionless slope-area (left) and steepness-curvature plots (right) of steady state topography using the *NoHyd* model. Area per contour width is used in place of area in both plots to maintain consistency with model formulation. The steepness-curvature relationship observed in the data show a precise fit to the linear relationship predicted from theory (dotted line). Parameters selected are the same as Figure 1Ai.

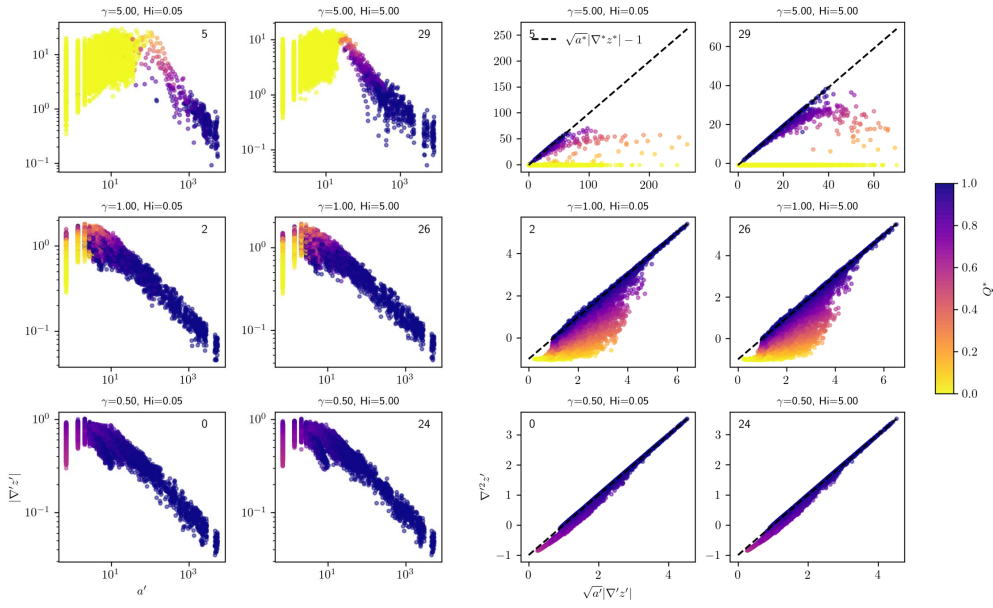


Figure 6. Dimensionless slope-area (left) and steepness-curvature (right) plots for selected model runs from Figure 2. See correlating numbers in the upper left corner. As in Figure 2, γ and H_i increase vertically and laterally from the bottom left respectively. Plots are colored by Q^* of the final topography. Axes scales are different between plots, showing that large γ cases obtain values of steepness and curvature far greater than the cases when γ is small.

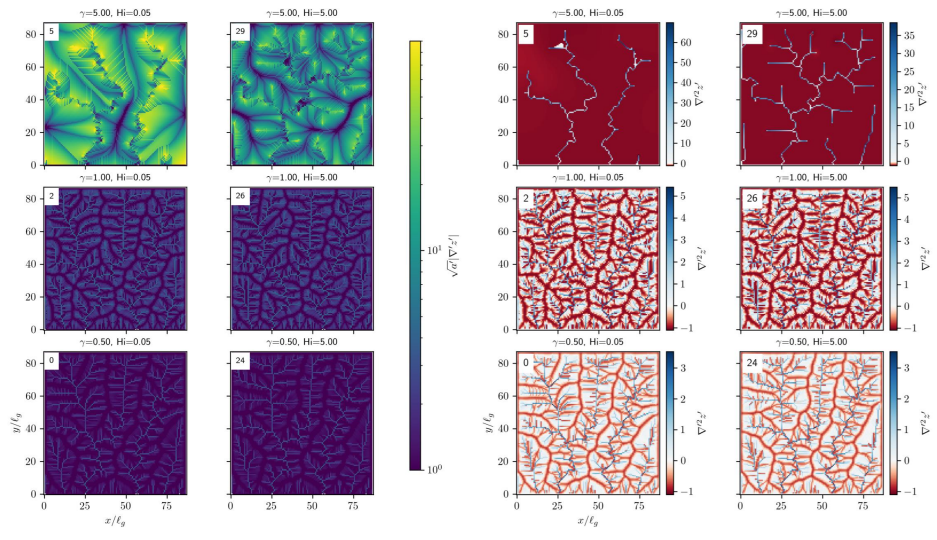


Figure 7. Planform view steepness and curvature for selected model runs, with run number corresponding to hillshades in figure 2. Spatial pattern of steepness appears to agree with channel network locations in the low γ cases, while in the high γ cases, it takes on large values in patterns that spiral away from ridges. Curvature is positive on ridges and negative in channels, with large areas of constant negative curvature in the large γ cases.

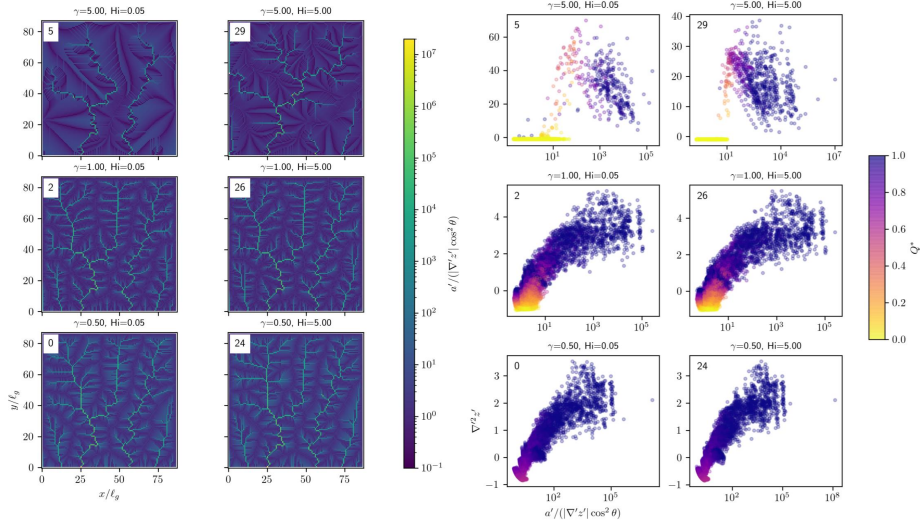


Figure 8. Planform view topographic index (left) and topographic index-curvature relationship for selected model runs, with run number corresponding to hillshades in figure 2

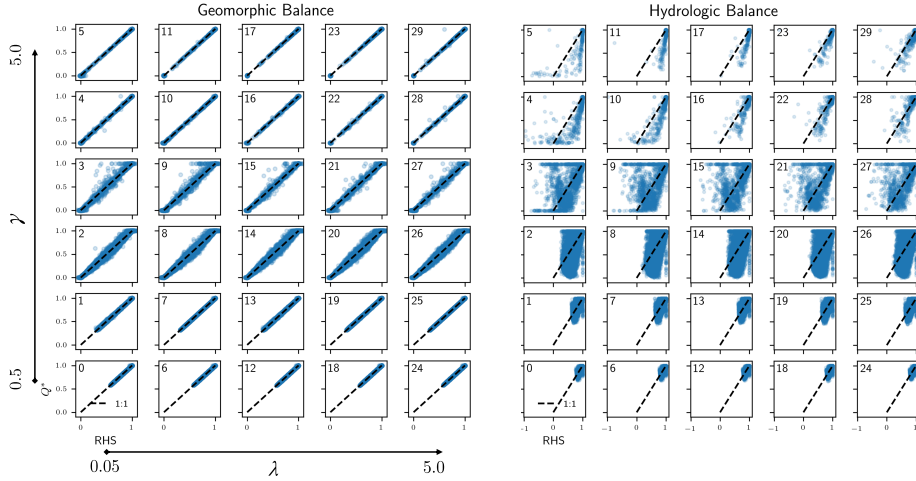


Figure 9. (A) Geomorphic balance from equation (62), plotting Q^* against the right hand side (RHS) of the equation. Subplots correspond to the same model runs as in 2. (B) Hydrologic balance from equation (70), plotting Q^* against the right hand side of the equation.

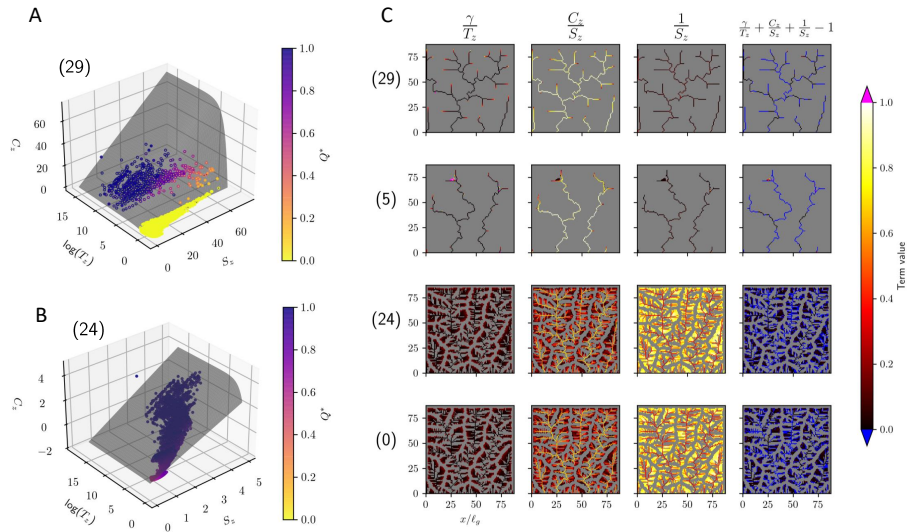


Figure 10. (A) Plot of the manifold (grey) defined in equation (73), with points plotted from model run (29), large H_i and large γ . The points in yellow are hillslope points, and lie on an approximately horizontal plane, not on the manifold. (B) Plot of the manifold defined in equation (73), with points plotted from model run (24), large H_i and small γ . (C) Map view of the terms of the hydromorphic balance in equation (73). Columns correspond to terms, with the final being the left hand side, which theory predicts to sum to zero. Rows are numbered with four different model runs with varying γ and H_i . Areas greyed out have $Q^* < 0.001$, thus representing hillslope points where the hydromorphic balance may not apply.

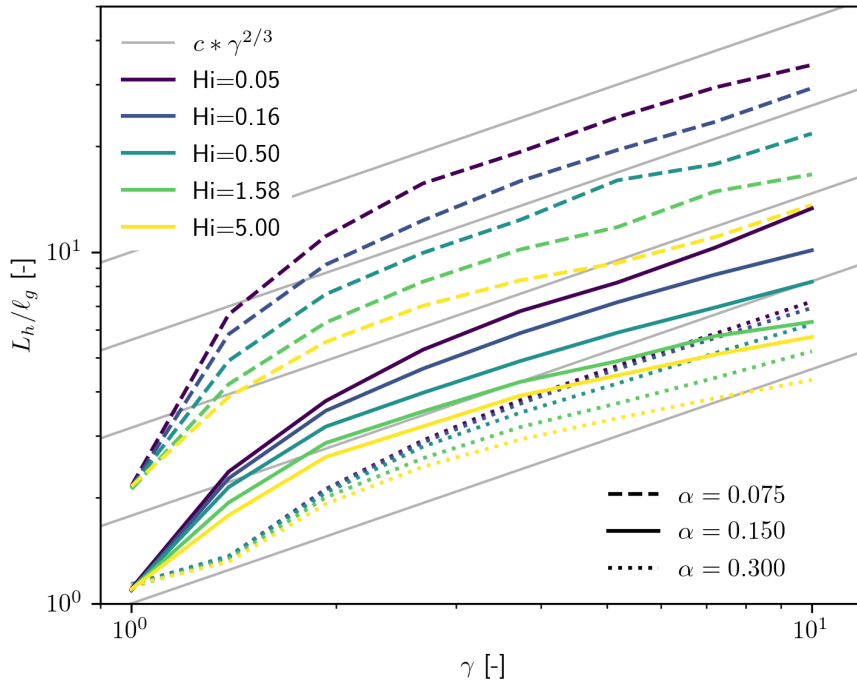


Figure 11. Hillslope length L_h increases with increasing γ . For a value of γ and α , L_h increases with decreasing Hi . Similarly, for a given value of γ and Hi , L_h increases with decreasing α . Gray lines with varying coefficients c show that the hillslope length scales approximately as $\gamma^{2/3}$ for $\gamma > 1$, which we derive from the hydromorphic balance.